T-3781

EXTENDED X-RAY ABSORPTION FINE STRUCTURE STUDIES OF Sn-RELATED DX CENTERS IN Sn-DOPED $Ga_{1-x}Al_xAs$

By

ABDELKADER OUTZOURHIT

ARTHUR LAKES LIBRARY
COLORADO SCHOOL of MINES
GOLDEN, COLORADO 8040'

ProQuest Number: 10783529

All rights reserved

INFORMATION TO ALL USERS
The quality of this reproduction is dependent upon the quality of the copy submitted.

In the unlikely event that the author did not send a complete manuscript
and there are missing pages, these will be noted. Also, if material had to be removed,
a note will indicate the deletion.

ProQuest 10783529

Published by ProQuest LLC (2018). Copyright of the Dissertation is held by the Author.

All rights reserved.
This work is protected against unauthorized copying under Title 17, United States Code
Microform Edition © ProQuest LLC.

ProQuest LLC.
789 East Eisenhower Parkway
P.O. Box 1346
Ann Arbor, MI 48106 – 1346

A thesis submitted to the Faculty and the Board of Trustees of the Colorado School of Mines in partial fulfillment of the requirements for the degree of Master of Science (Physics).

Golden, Colorado

Date: 08/09/89

Signed: A Outzourhit

Abdelkader Outzourhit

Golden, Colorado

Date: 9 Aug. 1989

Approved: T.M. Hayes

Dr. Timothy M. Hayes

Thesis Advisor

Golden, Colorado

Date: 8/14/89

F.D. Schowengerdt

Dr. F. D. Schowengerdt

Head of Physics Dept.

ABSTRACT

The local environment of Sn impurities in GaAs and $Ga_{0.7}Al_{0.3}As$ samples doped with $5x10^{18}$ cm^{-3} Sn has been investigated using extended x-ray absorption fine structure (EXAFS) spectroscopy at a temperature of ∿80 K. These samples are a factor of two to six more dilute than ones previously investigated using fluorescence detection. $ZnSnAs_2$ was used as a standard to assist in the analysis of the data for these samples. After an extensive comparison between the Sn nearest-neighbor peaks in these samples, it was found that the Sn atoms are tetrahedrally coordinated with As in GaAs and $Ga_{0.7}Al_{0.3}As$ (i.e., Sn occupies the group III sites). The Sn-As bond length in Sn-doped GaAs is 2.57 ± 0.02 Å, 0.12 Å greater than the Ga-As bond. The Sn-As bond length is found to increase by 0.03 Å from the shallow donor state in GaAs to the deep donor state in $Ga_{0.7}Al_{0.3}As$. These results support the small lattice relaxation model of the DX center.

TABLE OF CONTENTS

Abstract iii

List of figures vi

List of tables vii

Acknowledgments..viii

INTRODUCTION 1

PROPERTIES OF DX CENTERS 5

MODELS OF DX CENTERS 10

Large lattice relaxation 10

Small lattice relaxation..20

THEORY OF EXAFS SPECTROSCOPY 24

EXPERIMENTAL TECHNIQUE 33

X-ray source 35

Monochromator 35

Detectors 39

a. Transmission 39

b. Fluorescence 42

Data acquisition system 44

Experimental procedure 44

SAMPLES 46

DATA ANALYSIS 51

Addition of the data sets 51

Extraction of the EXAFS 52

Fourier transformation 55

Extraction of structural information 60

RESULTS AND DISCUSSIONS 67

EXAFS results for shallow Sn donors in GaAs 67

EXAFS results for Sn DX centers in $Ga_{0.7}Al_{0.3}As$. 75

Summary..85

RECOMMENDATIONS FOR FURTHER WORK 86

REFERENCES CITED 88

APPENDICES

A. Calculation of the resolution of the double crystal monochromator...............................92

B. Evaluation of sample thickness from the transmitted intensity 93

C. Calculation of nearest-neighbor distances in standards 94

List of Figures

Figure Page

1. LLR configuration-coordinate model for DX centers 12
2. MES data for $Ga_{1-x}Al_xAs$, x = 0 to 1 16
3. 2+3 fractional resonance vs Al mole fraction 17
4. Hall carrier concentration vs Al mole fraction 18
5. SLR configuration-coordinate model for DX centers 22
6. Schematic origin of EXAFS 26
7. Sn K-edge absorptance of $ZnSnAs_2$ 31
8. Sn K-edge absorptance of SnAs 32
9. Experimental arrangement...............................34
10. Schematic of the double crystal monochromator.........38
11. Arrangement of the detectors 41
12. Sn K-edge $k\chi$ of $ZnSnAs_2$ 56
13. Sn K-edge $k\chi$ of SnAs 57
14. Fourier transform of $ZnSnAs_2$ $k\chi$ 61
15. Fourier transform of SnAs $k\chi$ 62
16. Sn K-edge fluorescence yield of GaAs:Sn 68
18. Sn K-edge fluorescence $k\chi$ of GaAs:Sn 69
19. Fourier transform of GaAs:Sn $k\chi$ 71
20. Sn K-edge fluorescence yield of $Ga_{0.7}Al_{0.3}As$:Sn 76
21. Sn K-edge fluorescence $k\chi$ of $Ga_{0.7}Al_{0.3}As$:Sn 77
22. Fourier transform of $Ga_{0.7}Al_{0.3}As$:Sn $k\chi$ 80

LIST OF TABLES

Table Page

1. Activation energies of DX centers in $Ga_{1-x}Al_xAs$........7
2. Properties of the Si(400) double-crystal monochromator 37
3. Properties of the $Ga_{1-x}Al_xAs$ EXAFS samples............47
4. Lattice parameters for $ZnSnAs_2$, SnAs and GaAs.........49
5. Parameters used to extract $k\chi$ signals from $ZnSnAs_2$ and SnAs absorptances 58
6. Structural parameters of $ZnSnAs_2$ and SnAs 66
7. Parameters used to extract $k\chi$ from GaAs:Sn fluorescence yield 70
8. Structural parameters of Sn in GaAs 73
9. Parameters used to extract $k\chi$ from $Ga_{0.7}Al_{0.3}As$:Sn fluorescence yield 78
10. Structural parameters of Sn in $Ga_{0.7}Al_{0.3}As$: one-peak fits...81
11. Structural parameters of Sn in $Ga_{0.7}Al_{0.3}As$: two-peak fits...83

Acknowledgments

I would like to express my sincere appreciation to Dr. Timothy M. Hayes of the Colorado School of Mines for his continuous advice and endless patience without which this work could not have been completed. I would also like to thank Dr. D. L. Williamson for his remarks and discussions and for serving on my committee. I would like also to thank Dr. T. E. Furtak for being a member of my committee.

I am very grateful to the American Agency for International Development for the financial support. Special thanks to S. M. Bouldin and D. Durham of AMIDEAST for their continuous advice.

Special thanks to my family and all my friends for their continuous support.

Finally I would like to thank all the faculty and staff of the Physics Department at CSM.

To my parents and my brother Abdessalam who helped me through my academic career.

INTRODUCTION

The need for high speed electronic and efficient optoelectronic devices has stimulated research on a class of materials with very interesting electrical and optical properties. These are compounds of one or more elements from group III of the periodic table, such as Ga, Al, or In, with one or more elements from group V, notably As, P, or Sb. A key characteristic of III-V compound semiconductors, such as GaAs, that differentiates them from silicon is their direct band gap which leads to efficient electron-hole radiative recombination. In addition, the ability of III-V compounds to form solid solutions, such as the ternary semiconductor alloys $Ga_{1-x}Al_xAs$, makes it possible to obtain abrupt changes in the energy gap and in refractive index (Zee, 1982) by changing the Al mole fraction x, without affecting the lattice constant, a crucial consideration for epitaxial growth. A severe problem occurs, however, in association with n-type doping of alloys such as $Ga_{1-x}Al_xAs$, irregardless of the donor identity and the method of crystal growth. It has been found that, for Al mole fraction x greater than 0.22, deep levels with unusual properties are induced (Lang, 1985). These levels are called "DX centers", due to the observation that their concentration is proportional to the number of donors, and their electrical

and optical characteristics are not effective-mass-like (i.e, X for unknown defect). This defect degrades the performance of electronic and optoelectronic devices based upon these materials.

The microscopic models proposed for DX centers are of two types. They involve either a charge-state-controlled large lattice relaxation (Lang and Logan, 1977) or the effect of the host crystal band structure on the donor levels, with small or no lattice relaxation (Saxena, 1980). The lack of experimental atomic-scale structural information at the defect site has prevented either type of model from becoming widely accepted.

This work is part of an on-going research program on DX centers in which the Colorado School of Mines has been involved for several years in collaboration with the Laboratory for Solid State Physics and Solar Energy, C.N.R.S, in Valbonne, France. The objective of this program is to provide atomic-scale structural information about the defect and further to construct a microscopic model for this class of deep levels.

In the course of this program, epitaxial layers of $Ga_{1-x}Al_xAs$ (x = 0, 1) doped with ^{119}Sn-enriched Sn have been characterized by Mössbauer effect spectroscopy (Gibart et al., 1988). The study showed that two Sn species are present for the x = 0 sample: Sn atoms substituted for Ga (Sn_{Ga}),

which corresponds to the shallow donor; $Sn_{Ga}Sn_{As}$ pairs or Sn_3As_2-like clusters. The x = 1 sample yielded results that were interpreted in terms of two Sn sites: the shallow donor site Sn_{Al} and a clustered species (Gibart et al., 1988). These results were used to interpret the Mössbauer data for the x = 0.3 to 0.4 samples (Gibart et al., 1988). The measured spectra showed new Sn sites with highly localized electrons, and were ascribed to one, two or even a distribution of DX centers, with a distortion from tetrahedral symmetry around the donor site. The magnitude of the distortion, however, was not estimated.

The objective of the present work is to probe the local environment of the Sn atoms in $Ga_{1-x}Al_xAs$ using x-ray absorption spectroscopy (XAS). Specifically, we will analyze the post-edge oscillations occurring in the absorption coefficient of an atom in a solid, known as the extended x-ray absorption fine structure (EXAFS). This technique has proved to be very powerful in probing the local environment of specific atoms in dilute as well as concentrated systems (Hayes and Boyce, 1982). Sn K-shell fluorescence EXAFS experiments were performed on Sn-doped $Ga_{1-x}Al_xAs$ with Al mole fraction x = 0 and 0.3. The Sn atom is expected to be in a shallow donor state in GaAs and in a deep state predominantly for x ranging from 0.3 to 0.4 at low temperatures. The present work will attempt to

clarify whether large or small lattice relaxations are involved in the formation of the DX centers.

PROPERTIES OF DX CENTERS

Deep levels responsible for persistent photoconductivity (PPC) at low temperatures in n-GaAsP were reported twenty-two years ago (Garford et al., 1968). Similar effects were observed in n-type AlGaAs (Nelson, 1977), and subsequently called DX centers (Lang et al., 1979) presuming that the deep level is a complex involving the donor atom (D) and an unknown defect (X). The essential features of this class of deep defects are summarized below.

(i) They are present in n-type $Ga_{1-x}Al_xAs$ for $x > 0.22$ irrespective of whether the donor dopant is on a III-site (Si, Sn), or on a V-site (Se, Te), and independent of the method of growth: liquid phase epitaxy (LPE), metal-organic vapor-phase epitaxy (MOVPE), or molecular beam epitaxy (MBE). The concentration of DX centers is proportional to that of the donors (Lang, 1985).

(ii) They are responsible for carrier freeze-out at low temperatures ($T< 100$ K) and persistent photoconductivity (PPC). They also reduce the carrier concentration at room temperature and the radiative recombination efficiency.

(iii) The DX center is the dominant electron trap for $x >0.22$. Both electron emission from and capture by the DX center are thermally activated (Lang and Logan, 1977). This leads to device instabilities and noise at room temperature.

Table 1 shows the activation energies of the DX centers associated with different donors (Lang, 1985). The carrier concentration activation energy found by Hall measurements for Sn-doped $Ga_{1-x}Al_xAs$ is $E_o \approx 0.1$ eV, increasing slowly with x (Lang, 1985). In contrast the activation energy for emission of an electron from a bound state to a free state, found from nonequilibrium measurements such as deep level transient spectroscopy (DLTS), is $E_e = 0.19$ eV and is constant. The difference represents the energy barrier E_b to thermal capture of a free electron from the conduction band minimum to the DX center and is consistent with the observed persistent photoconductivity (PPC) (Lang and Logan, 1977). The optical excitation energy E_n is, however, on the order of 1.1 eV, corresponding to the maximum in photoconductivity.

(iv) The first microscopic structural information concerning the defect site was derived from the selection rules for the attenuation of ballistic phonons (Narayanamurti et al., 1979). The results revealed a strong attenuation of the ballistic phonons in the <111> direction for ionized Sn DX centers and for the $0 < x < 0.22$ samples in dark. The attenuation was not observed when the DX centers are occupied. These observations led the authors to suggest a trigonal local symmetry for the DX centers associated with Sn-doped samples and orthorhombic for

Table 1. Activation Energies of DX centers in $Ga_{1-x}Al_xAs$ [1].

Donor Impurity	E_e (eV)	E_b (eV)	E_o (eV)	E_n (eV)
Se	0.28	0.18	0.1	0.85
Te	0.28	0.18	0.1	0.85
Si	0.43	0.33	0.1	1.25
Sn	0.19	0.09	0.1	1.1

E_e is the activation energy for thermal emission of an electron from the ground state of the DX center

E_b is the thermal barrier for recapture of a free electron

E_o is the Hall activation energy

E_n is the optical ionization energy.

1. Lang 1985.

Te-doped ones (Narayanamurti et al., 1979). This interpretation assumes, however, that the observed distortions for the ionized DX center are consistent with the stable position for the occupied defect. Subsequent EXAFS measurements on Se-doped $Ga_{0.62}Al_{0.38}As$ revealed no lattice distortion (Kitano and Mizuta, 1987). More recently, Mössbauer effect spectroscopy (MES) measurements on Sn-doped $Ga_{1-x}Al_xAs$ (with x varying from 0 to 1) suggest a distortion from tetrahedral symmetry at the impurity site (Gibart et al., 1988).

(v) A deep level attributed to the DX centers appears in Si or Sn-doped GaAs at high pressure. This effect was observed using different experimental methods: DLTS (Mizuta et al., 1985), photoconductivity (Tachikawa et al., 1985), and Shubnikov-de-Haas effect (Maude et al., 1985). These measurements showed that, in addition to the shallow donor, a deep level appears under hydrostatic pressure larger than 24 Kbars. Such results support the argument that the occurrence of the DX center is related mainly to the progressive change in the band structure of $Ga_{1-x}Al_xAs$ as x is increased.

vi) It was recently reported that DX centers are also present in $Ga_{1-x}Al_xAs$ for $x < 0.22$. The level in this case is resonant with the Γ conduction band minimum and can be populated by exciting the electrons with an electric field

(Theis et al., 1986). The level can be brought deep into the gap by applying hydrostatic pressure as in the case of GaAs. Theis et al. (1987) have found that DX centers are also present in heavily n-type doped GaAs ($N_d > 5x10^{18}$ cm^{-3}) as resonance states in the conduction band.

vii) More recently, Mizuta et al. (1988) found, through photo-Hall measurements, that both shallow and DX centers exist in the indirect band gap regime of $Ga_{1-x}Al_xAs$ (x> 0.45). The observed PPC, however, was much smaller as a consequence of the deepening of the shallow state (Mizuta et al., 1988).

ARTHUR LAKES LIBRARY
COLORADO SCHOOL of MINES
GOLDEN, COLORADO 80401

CURRENT MODELS FOR DX CENTERS

Microscopic models for DX centers must explain their electronic and optical properties. The electronic properties of shallow impurities are well understood on the basis of the effective-mass theory. Extensions of this theory have been made to moderately deep levels using more realistic impurity potentials and pseudopotentials (Lannoo and Bourgoin, 1981). The DX center, however, has energy levels very deep in the gap and a wave function which is very localized in the vicinity of the impurity. Effective-mass theory is not adequate for such defects. Several microscopic models have been proposed for DX centers. These models are subdivided into two classes as discussed below: those incorporating a large lattice relaxation and those with a small lattice relaxation.

Large Lattice Relaxation (LLR)

The introduction of an impurity (point defect) induces displacements of the first, second, etc., neighbors, depending on the range of the perturbation introduced by the defect. The type of the distortion depends on the way the defect is bonded to the neighboring atoms and thus on the charge state of the defect (Lang and Logan, 1977). To account for the PPC, Lang and Logan (1977) proposed that

both thermal capture and emission are thermally activated. This results in a small capture cross section for the defect at low temperatures. The observation that the photo-ionization energy is much larger than the activation energies for both emission and capture suggests a large energetic charge-state-controlled lattice relaxation, leading to a strong coupling between the electronic and the vibrational states of the defect. Lang and Logan (1977) also proposed a configuration coordinate diagram for the defect in this large lattice relaxation (LLR) limit similar to the one presented in figure 1. It is consistent with the experimental values of the activation energies. The vibration of the defect is represented by a single configuration coordinate Q and by a force constant $k=M\omega^2$ where ω is the energy of the phonon involved in the coupling, and M is the reduced mass of the defect. The electron-phonon interaction was taken to be linear in Q. The lattice relaxes to $Q=Q_T$ when the electron is captured by the DX center. The optical ionization energy is related to the Hall activation energy by $E_n=E_0+S\hbar\omega$, where $S\hbar\omega$ is the lattice relaxation energy and S is the Huang-Rhys factor (Lang, 1985).

The LLR was ascribed to a complex involving the donor and an anion vacancy (V_{As}) (Lang et al., 1979). Subsequently, a measurement of the attenuation of ballistic

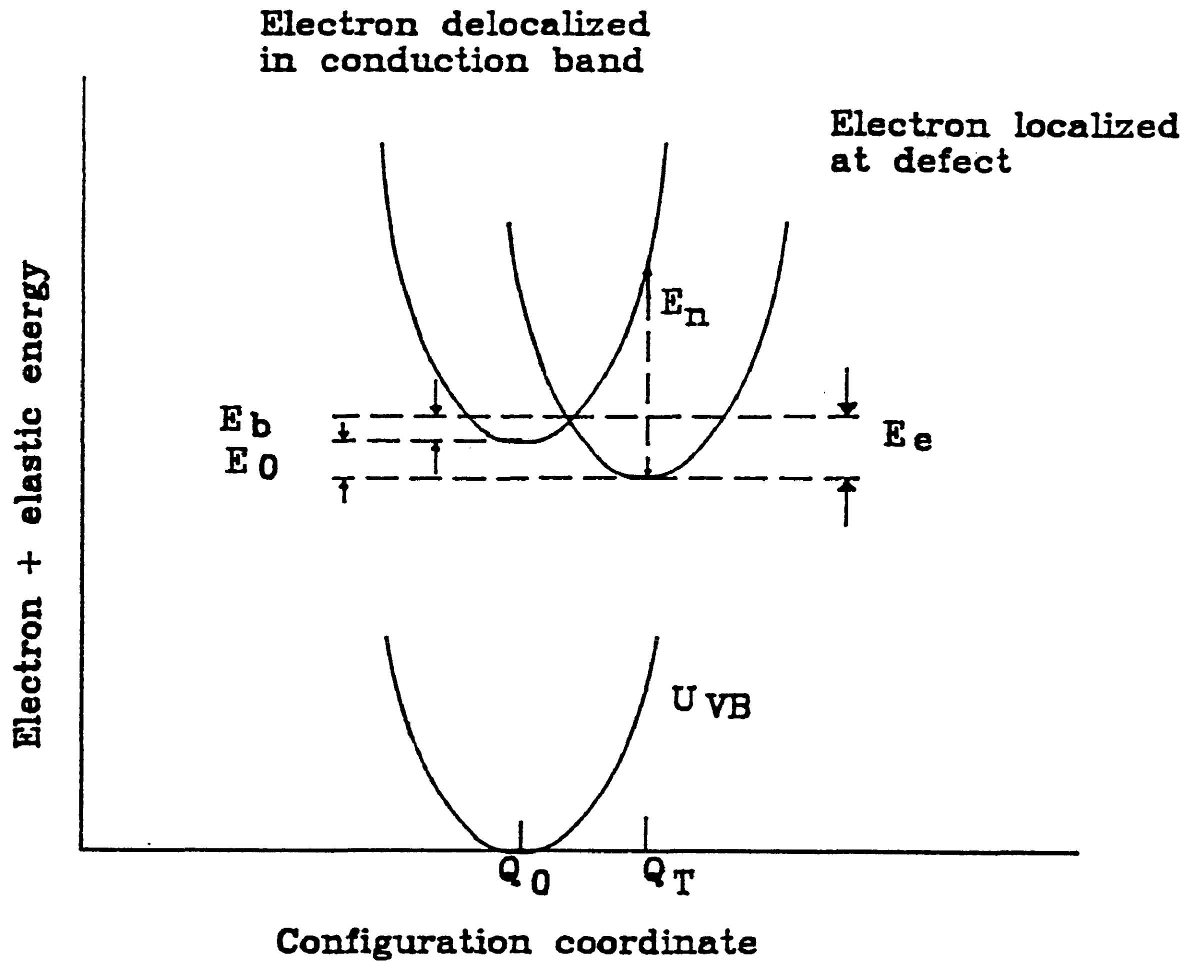

Figure 1. LLR configuration coordinate model of the DX center (reproduced from Henning and Ansem (1987)).

phonons by Narayanamurti et al.(1979) provided evidence for a reduction of local symmetry at the DX center, and was used to support the argument that the defect is due to a Sn-V_{As} nearest-neighbor complex in Sn-doped $Ga_{1-x}Al_xAs$ and a Te-V_{As} second-nearest-neighbor complex in Te-doped samples. An argument against these models is that the crystal growth methods for $Ga_{1-x}Al_xAs$ operate at high As vapor pressure, which makes it highly unlikely that a substantial number of As vacancies would be available to form such a high concentration of donor-vacancies. In addition, the hot electron measurement of Theis et al.(1986) supports the argument that the DX center involves the donor only and differs from the shallow state by a change in local lattice configuration. Theis et al. (1984) also showed by far infrared measurements that the ionized DX center acts like a shallow donor.

A model based upon the effect of alloy disorder on sp^3 bonding was proposed in the indirect band gap regime (Uchida et al. 1985). The anisotropic distribution of Al and Ga atoms results in instability of the sp^3 bonding between the donor and the host atoms, resulting in bond reconstruction into sp^2- or even sp-like bonding. The DX center is formed by a large shift of the impurity from its central position, and the shallow-to-DX transition is due to bond reconstruction from sp^3 to more stable ones (Uchida et al.

1985).

Another LLR model is supported by Morgan (1986) who suggested that the DX center is derived from the T_2 effective-mass state linked to the L valleys. The defect was suggested to be due to the displacement of the donor from its centered lattice position, a Jahn-Teller-like effect, the nature of which was explained as follows. The DX center is derived from a triplet of symmetry T_2, which is formed by the four nearest neighbor antibonding orbitals. One component of this state has a symmetry axis along one of the <111> directions and thus 75% of the electron probability density lies along this axis and only 25% along the other three, displacing the donor in the <111> direction away from one neighbor towards the other three by an amount which lowers the total energy of the state. This class of instabilities does not involve energy barriers, but does results in a decrease of the energy of the degenerate state.

A discrete variational $X\alpha$ cluster calculation for Si-doped $Ga_{1-x}Al_xAs$ was carried out by Oshiyama et al. (1987). In their model for an undistorted cluster (as in GaAs), the antibonding state of symmetry A_1 forms a resonance state in the conduction band. The strain field caused by partially replacing Ga by Al triggers a distortion

of the nearest-neighbor As atoms around Si. This shifts the antibonding level deep into the gap. The authors argued that this level is the DX center.

Recent Mössbauer Effect Spectroscopy (MES) measurements on Sn-doped $Ga_{1-x}Al_xAs$ samples prepared under the same conditions as the ones under study here have supported a LLR model (Gibart et al., 1988). The results for the x = 0, 0.2, 0.3, 0.4, 0.43, 0.76, and 1 samples are presented in figure 2. For the x = 0 sample (GaAs), resonance line 1 was identified as originating from the substitutional shallow donor Sn site, Sn_{Ga}. The resonance lines 2 and 3 were attributed to $Sn_{Ga}Sn_{As}$ pairs or Sn_3As_2 microprecipitates (Williamson, 1986). For the x = 1 sample (AlAs), the Mössbauer resonance line 1 was attributed to the shallow donor Sn site, Sn_{Al}. Lines 2 and 3 are due to electrically inactive clustered Sn species (Gibart et al., 1988). The increase in the signal from resonance lines 2 and 3 for x between 0.3 and 0.4 was attributed to the DX centers based upon correlating the fractional resonance intensity of these lines with the variation of the concentration of DX centers, their activation energies, and the Hall carrier concentration with the alloy composition. This fraction (figure 3) peaks near x = 0.3 to 0.4 where the Hall carrier concentration is a minimum (figure 4). The authors found a strong localization of the electron density at the Sn site

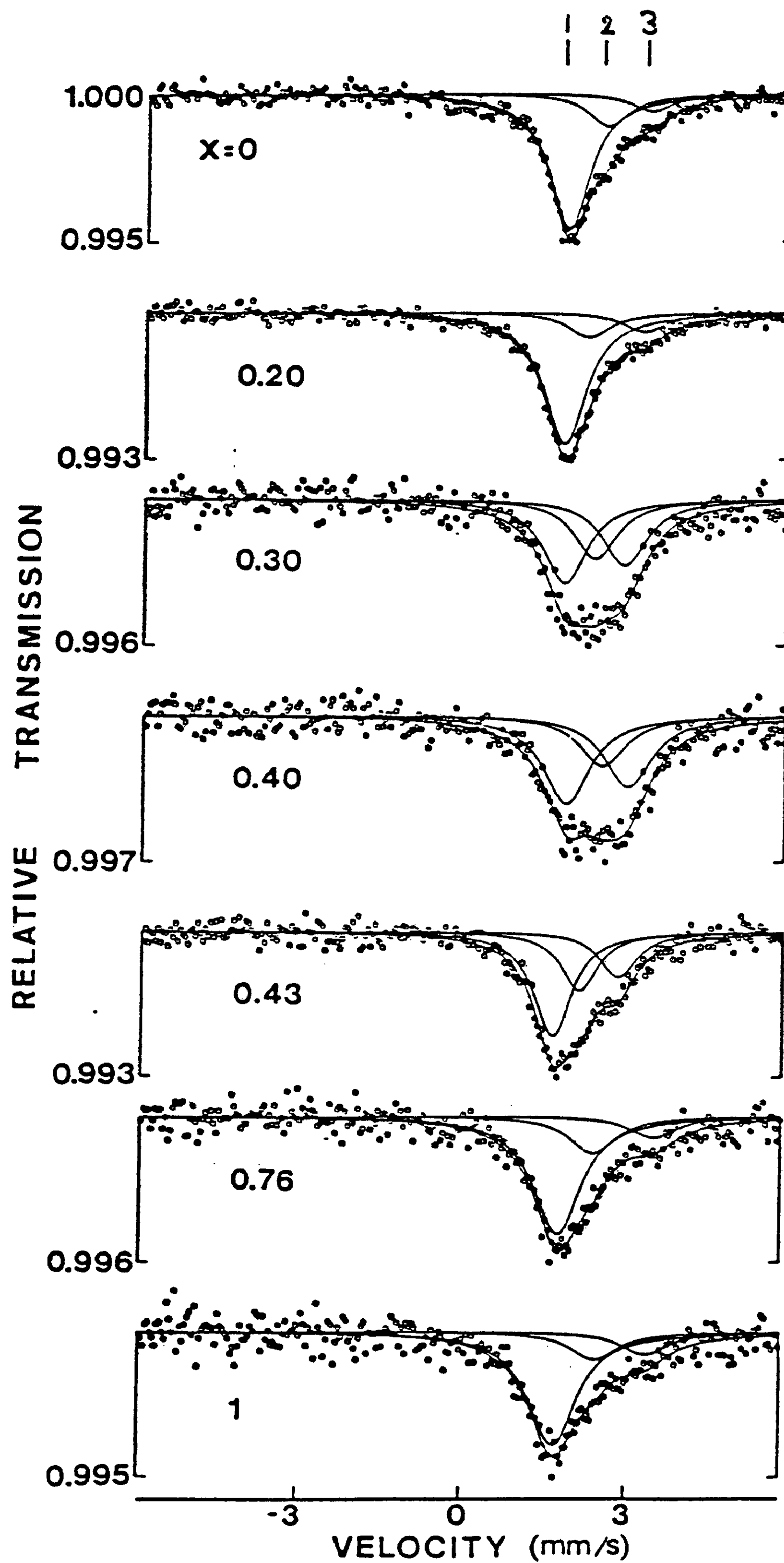

Figure 2. MES spectra for $Ga_{1-x}Al_xAs$ (x=0 to 1). The solid line through data points is a fit of the three Lorentzian lines indicated (Gibart et al., 1988).

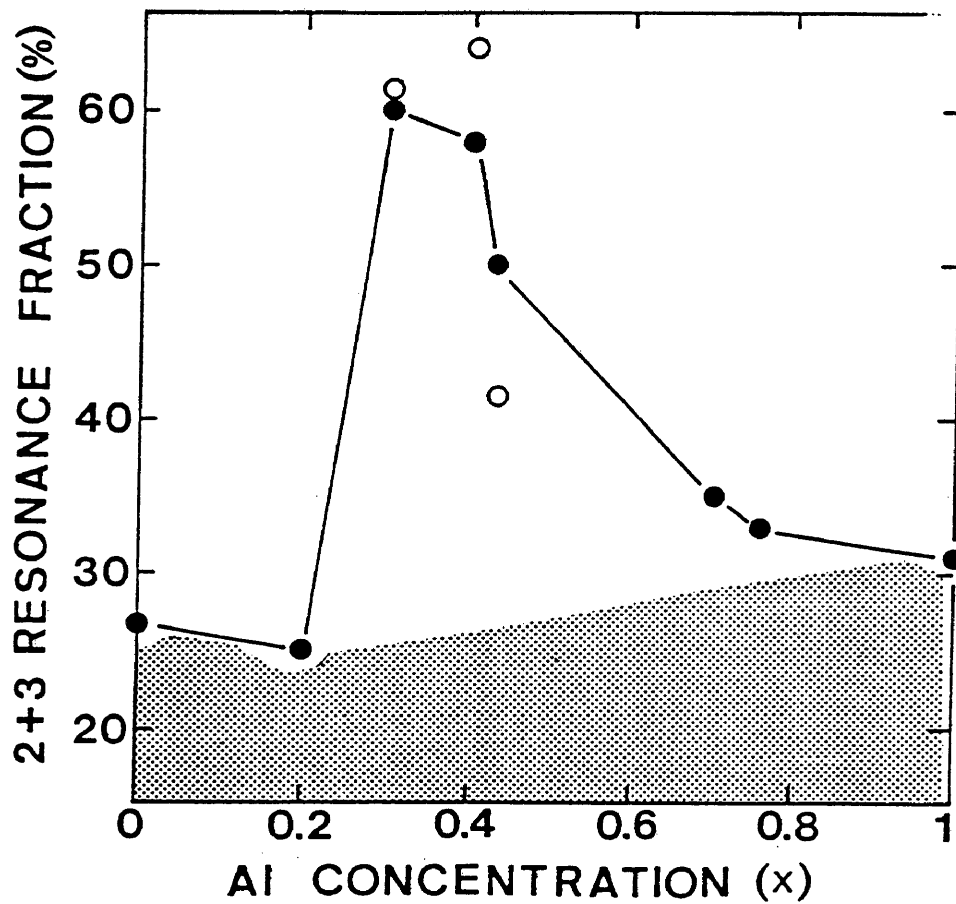

Figure 3. 2+3 fractional resonance vs Al mole fraction. Region above shaded area is attributed to DX centers (Gibart et al., 1988).

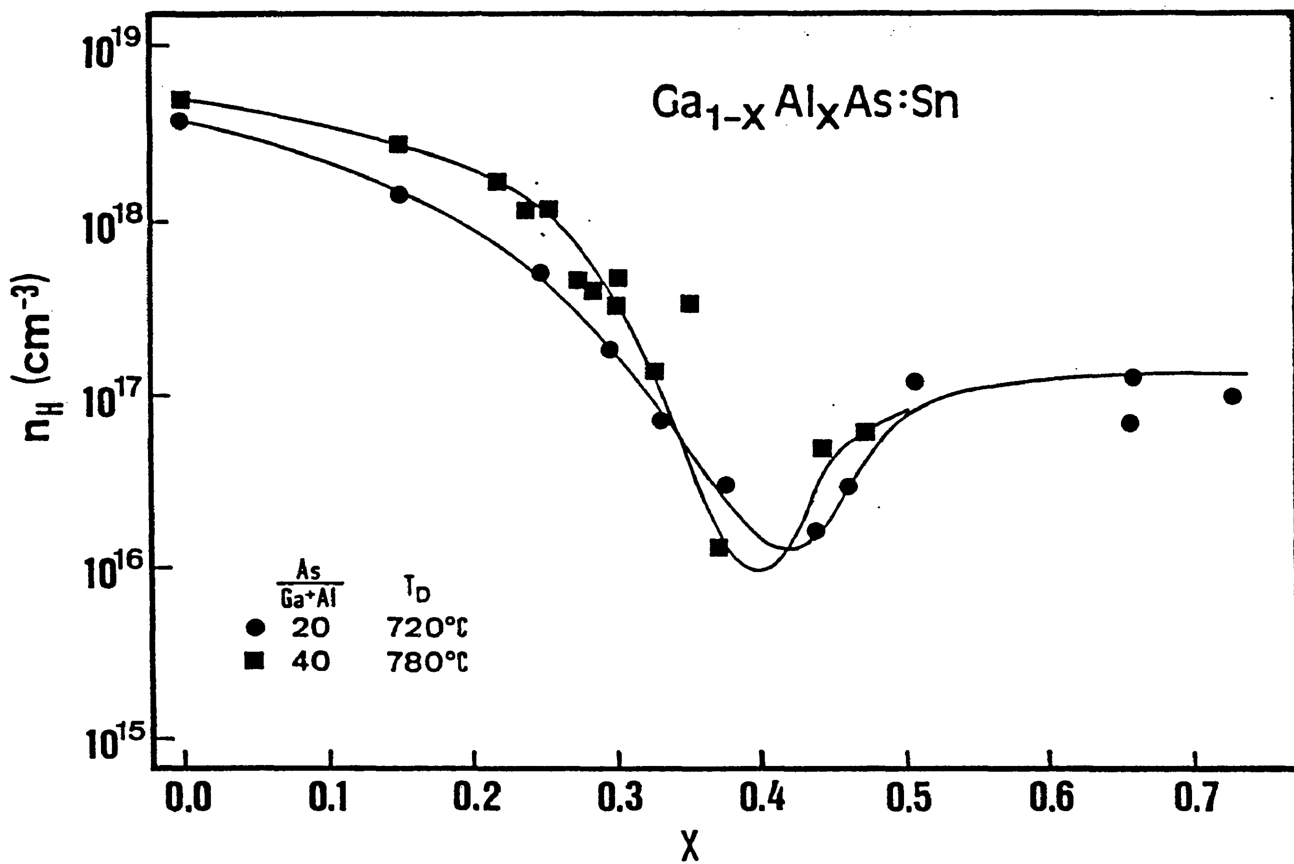

Figure 4. Hall carrier concentration vs Al mole fraction for two Sn-doped samples (Gibart et al., 1988).

as detected by the Mössbauer isomer shift of the DX resonance. The authors argued that these results are compatible with one, two, or even a distribution of DX centers, with a distortion of the cubic symmetry around the donor. The magnitude of the distortion, however, is difficult to establish due to the lack of a simple relation between it and the quadrupole splitting.

Khachaturyan and Weber (unpublished), on the other hand, proposed a quasipolaron model for DX centers in $Ga_{1-x}Al_xAs$, which was suggested to be an antibonding electron self-trapped on a trigonal (C_{3v}) distortion of the nearest-neighbor tetrahedron of the donor. The distortion was proposed to originate from asymmetric displacement modes of the impurity atom, and be stabilized by the trapped antibonding electron. This extrinsic self-trapping model was originally due to Toyozawa for an electron moving in a deformable lattice (see Toyozawa and Shinozuka, 1980, and references therein).

Chadi and Chang (1988), suggested that the DX center is a negatively charged center (negative U) resulting from the reaction:

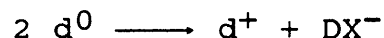

$$2\ d^0 \longrightarrow d^+ + DX^-$$

The authors argued that the defect formation results from a bond-rupturing displacement of the impurity along a bond axis by 1.17 Å (for Si), into a threefold coordinated

interstitial site (Chadi et al., 1988). The negative-U model is supported by the absence of any electron paramagnetic resonance signal from the defect (Khachaturyan et al., 1988). Theis (1988) favors this model in a recent review. A recent high-pressure MES study of ^{119}Sn-doped GaAs suggests that two or three electrons are localized in the ground state of the DX center (Gibart et al., 1989).

Small Lattice Relaxation Models

The band structure of $Ga_{1-x}Al_xAs$ is well established experimentally and theoretically. As x is varied from 0 to 1, the band gap increases from 1.4 eV (direct) to 2.2 eV (indirect), the crossover occurring at $x = 0.45$. Both column IV and VI dopants give rise to donor levels which tend to track the L conduction band minimum (Theis, 1986). The activation energy of the level measured from the conduction band minimum, $(E_\Gamma - E_{DX})$, follows the L band edge. Extrapolation of the data to $x < 0.22$ demonstrates that the level lies above E_Γ and thus forms a resonant state with the Γ conduction band minimum (Theis, 1986). As observed by Mizuta et al. (1985) in Si doped $Ga_{1-x}Al_xAs$ at low Al mole fractions, including GaAs, this level can be brought deep into the gap by applying hydrostatic pressure. The level can also be persistently populated by exciting the electrons with an electric field (Theis et al., 1986).

These observations suggest that the DX is present in n-type doped GaAs as well as in $Ga_{1-x}Al_xAs$, the level being metastable for $x < 0.22$ and stable for $x > 0.22$. This is further confirmed by the most recent observation of Mizuta el al. (1988) that DX centers exist in the indirect band gap regime. All these results support the argument that the DX centers derive much of their characteristics from the band structure of the host crystal.

One of the earliest such models involving small or no lattice relaxation (SLR) was due to Saxena (1980), who suggested a deep donor 0.2 eV below the L valleys. The PPC was explained as follows: upon ionization, the DX center is promoted to the L valley and reaches the Γ band minimum via intervalley scattering. The recapture by the deep level is inhibited by symmetry. In the small lattice relaxation limit, the crossover of the adiabatic potentials occurs at small values of the configuration coordinate as depicted in figure 5 (Henning and Ansems, 1987).

The SLR model is supported by the work of Yamaguchi (1986, 1987), who proposed a theoretical model based upon the scattering theoretic method (STM) and an empirical sp^3s^* tight-binding Hamiltonian. He argued that the DX center is of A_1 symmetry (i.e., symmetric distortion) and is due to the central cell potential attributed to the defect and its four nearest neighbors. The change in the bond length was

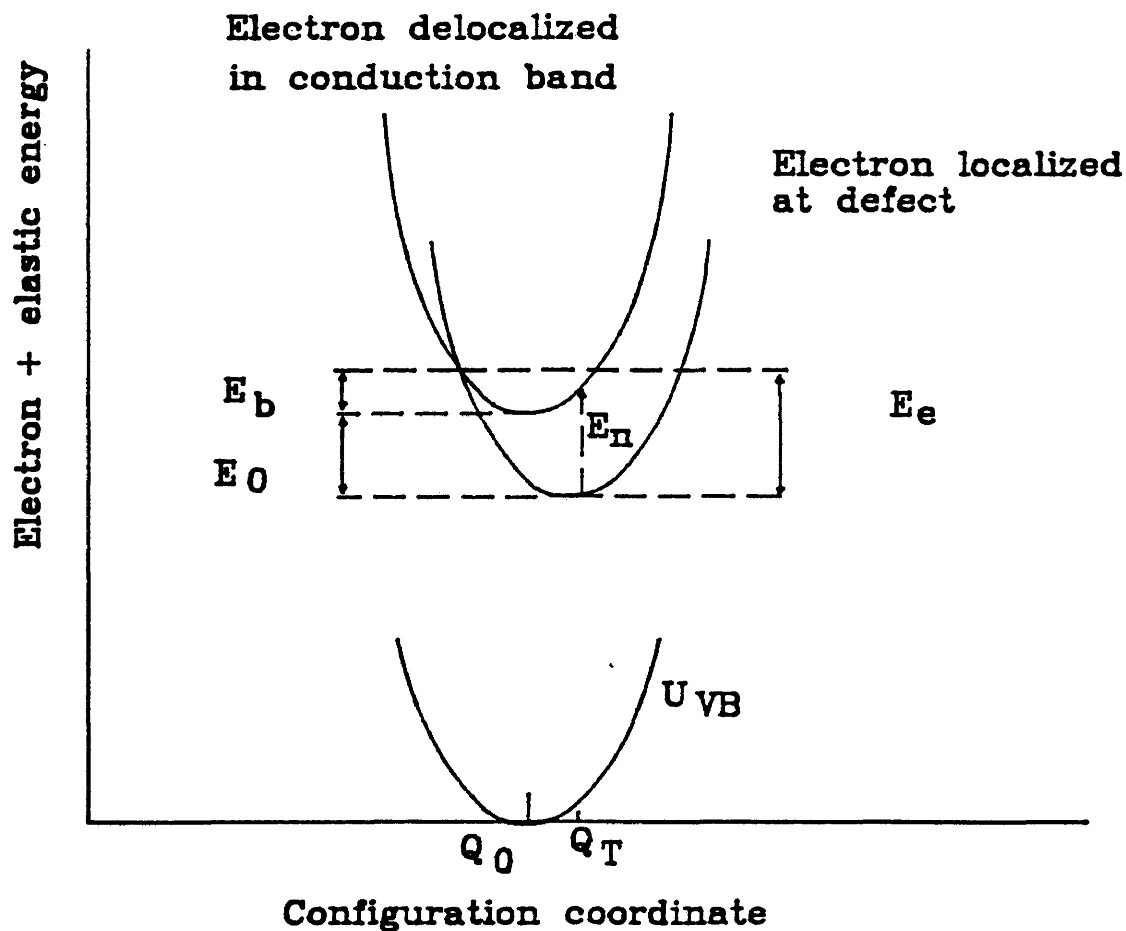

Figure 5. SLR configuration coordinate model of the DX center (Henning and Ansem, 1987).

estimated to be -0.3 Å for Si and 0.15 Å for Sn donors.

The first direct structural measurement was due to Kitano and Mizuta (1987, 1988) using EXAFS spectroscopy. Measurements on Se-doped $Ga_{0.62}Al_{0.38}As$ revealed no significant bond length change (less than 0.04 Å) between the two donor states. The concentration of donors in these samples was quite high, however, ranging from 1 to $3x10^{19}$ cm^{-3}, probably resulting in predominantly clustered species and precipitates. This can be seen clearly from their data for the PPC state, which shows a carrier concentration less than their nominal doping densities.

The microscopic structure of the DX center is a critical component of any microscopic model, but is still an open subject. Given the technological importance of these materials, we addressed this need with a series of x-ray absorption spectroscopy structural measurements on Sn-doped $Ga_{1-x}Al_xAs$.

THEORY OF EXAFS SPECTROSCOPY

The objective of the present work is to obtain detailed structural information at the defect site using the extended x-ray absorption fine structure spectroscopy (EXAFS) spectroscopy, which has proven to be a powerful probe of microscopic local structures. To this end Sn K-shell fluorescence EXAFS data were acquired for Sn-doped $Ga_{1-x}Al_xAs$ (x=0, 0.3) samples at low temperatures, allowing the characterization of the two states of Sn atoms in $Ga_{1-x}Al_xAs$: shallow donor state in GaAs:Sn; predominantly DX state for x=0.3 at 77 K. Data were also taken for different standards needed to analyze the data: $ZnSnAs_2$ in which each Sn atom is surrounded by four As atoms in a tetrahedral coordination; SnAs in which the six neighboring As atoms have an octahedral coordination.

X rays are absorbed by matter mainly through the photoelectric effect. As the x-ray photon energy is increased, the more tightly bound atomic core electrons can be excited. The onset of excitation of the K-shell electrons, for example, is marked by an abrupt increase in absorption called the K-edge. The post-edge oscillations in the absorption coefficient of an atom embedded in a solid are referred to as the extended x-ray absorption fine structure or EXAFS. Figure 6 shows the origin of this

effect. The x-ray photon is absorbed by an atom through the ejection of an electron from a core state j to unoccupied continuum state f. The photoelectron wave in the core region is the sum of an outgoing part of the wave and a part that is scattered back from the neighboring atoms. The interference between these waves modulates the absorption cross section of the excited atom. The phase difference between these two waves is given by the sum of the following contributions: the distance traveled by the photoelectron times the wave number; twice the phase shift due to the excited atom plus the phase shift due to the potential of the scattering atoms. The oscillations result from the dependence of the phase difference upon the energy of the incident x rays, through the photoelectron wave vector given by (Hayes and Boyce, 1982)

$$k = \sqrt{\frac{2\ m}{\hbar^2}\ (\ E - E_0)} \quad ,$$

where E is the final-state electron energy. E is related to the energy of the incident x rays for a K-shell excitation by

$$E = E_{1s} + \hbar\omega,$$

where E_{1s} is K-shell binding energy, and E_0 is the final-state electron energy corresponding to zero momentum.

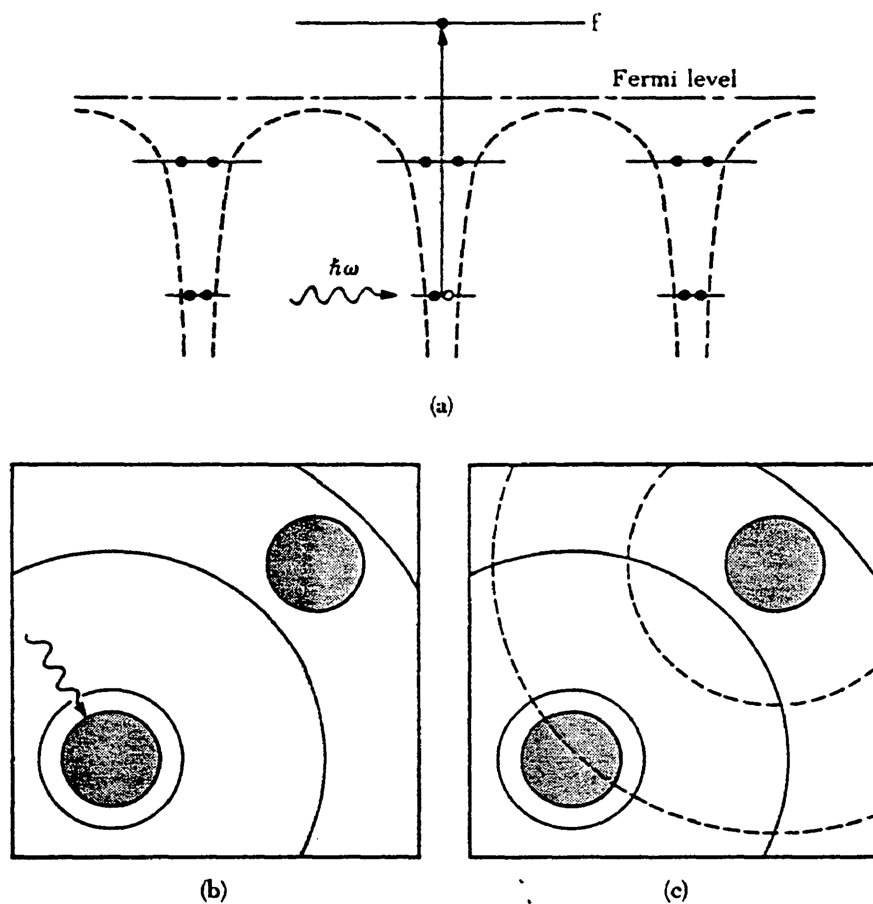

Figure 6. Schematic origin of EXAFS (Hayes and Boyce, 1982).
a. Photoionization.
b. Outgoing photoelectron wave.
c. Scattered wave from neighboring atom interferes with the outgoing wave at the excited atom.

k and thus the net phase vary as a function of photon energy. This results in a change in the final state of the photoelectron, and thus in the post-edge oscillations in the absorption spectrum of the excited atom. The frequency of the oscillations contains information about the near neighbor distances.

The theory of EXAFS is well established and has been well documented (see Hayes and Boyce, 1982, and references therein). A more accurate approach than the one presented above accounts for scattering of the photoelectron by more than one atom as well as multiple-electron excitations. Each multiple-atom scattering event, however, can be described by an effective interference path length equal to the sum of the scattering paths. The contributions from such processes will not interfere with the nearest-neighbor (nn) peak of interest here. In addition the near edge structure, which contains the principal contributions from multiple-atom scattering, is always discarded when Fourier transforming the data into r-space. The multiple-electron excitations result in a distribution of photoelectron momenta, causing a spread in phase, and tend to cancel one another (Hayes and Boyce, 1982, Lee et al., 1981). These contributions can therefore be neglected. Under these assumptions, the problem is reduced to the scattering of the photoelectrons by atoms.

The absorption cross section for the photoexcitation of an electron from the K-shell of atom species α is then given by (Hayes and Boyce, 1982)

$$\sigma_\alpha(\omega) = \sigma_\alpha{}^0(\omega)(1 + \chi_\alpha(\omega)),$$

where $\sigma_\alpha{}^0(\omega)$ is a free atom-like absorption cross section, which is smoothly varying in the pre- and post-edge regions and has a step at the absorption edge of the excited atom, and $\chi_\alpha(\omega)$ is the single-atom scattering EXAFS given by (Hayes and Boyce, 1982)

$$k\chi_\alpha(k) = \sum_\beta \int_0^\infty p_{\alpha\beta}(r)/r^2 \; 2\mathrm{Re}[\exp(2ikr)\Lambda_{\alpha\beta}(k,r)] \, dr \; ,$$

where

$$\Lambda_{\alpha\beta} \simeq - \left[\frac{2i\pi^2 m}{\hbar^2}\right] t_\beta(-\mathbf{k},\mathbf{k}) \; \exp[-2r/\lambda(k) + 2i\eta_\alpha(k)] \; .$$

In these expressions, k is the momentum of the final-state electron, $p_{\alpha\beta}(r)$ is the radial distribution of atom species β around the central atom α, normalized to the number of atom species β in the sample. The scattering term $\Lambda_{\alpha\beta}$ accounts for the interaction of the final-state electron with the excited atom, the backscattering atoms, and the whole solid. These interactions are expressed, respectively, in the $l = 1$ phase shift η_α due to the potential of the excited atom, the t-matrix of the backscattering atoms

$t(-\mathbf{k},\mathbf{k})$, and the electron mean free path λ due to inelastic scattering effects. This scattering term contains information about the identity of the near neighbors.

The structural information in the EXAFS is in the pair distribution $p_{\alpha\beta}(r)$, which peaks at the near neighbor distances. For the case of a Gaussian distribution of N_j atoms at a mean distance r_j around the central atom, the contribution of that shell to the EXAFS signal is given by (Hayes and Boyce, 1982)

$$k\chi_j(k) = \frac{2N_j}{r_j^2} |\Lambda(k,r_j)| \exp(-2(\sigma_j k)^2) \cos(2kr_j+\Phi_j),$$

where σ_j is the half width of the distribution and Φ_j is the total phase shift. From this expression, it can be seen that the Fourier transform $\phi(r)$ of the EXAFS signal $k\chi(k)$ peaks nearly at the nearest neighbor distances r_j where the pair distribution peaks. The linear term in the Φ_j shifts the peaks slightly from r_j. The amplitude of the peak is proportional to the number of near neighbors and decreases for more distant neighbors due to thermal and/or static disorder, and inelastic scattering effects. The goal of the data analysis is to extract the pair distribution function $p(r)$ from $\phi(r)$, and thus the nn distance, the coordination number, the type of neighbors, the mean square deviation from r_j.

Figures 7 and 8 show respectively the Sn K-edge absorptance of $ZnSnAs_2$ and SnAs. The temperature of the samples ranged from 80 to 90 K. The sharp increase in the absorptance corresponds to Sn K-shell absorption edge ($\sim$29.2 KeV). The oscillations start above the edge in both cases and continue to the upper limit of the data range. The experimental technique and the data analysis will be discussed in the following sections.

In applying this technique, it should be borne in mind that photo- as well impact-ionization of DX center can occur. The question arises then as to whether the irradiation from the x-ray beam and collisions with the photoelectrons or Auger electrons accompanying the absorption break down the DX state, producing the shallow (ionized) state. To this end, Mizuta and Kitano measured the change in capacitance of their Se-doped $Ga_{0.62}Al_{0.38}As$ using monochromatic Cu x rays. An increase in the capacitance was observed at 70 K. The shallow donor concentration calculated from C-V characteristics, however, was found to be less than 10^{17} cm^{-3} which is negligible compared to the doping levels of their samples (on the order of 1 to 3×10^{19} cm^{-3}). This suggests that the DX center is the dominant state at low temperature during x-ray irradiation.

ARTHUR LAKES LIBRARY
COLORADO SCHOOL of MINES
GOLDEN, COLORADO 80401

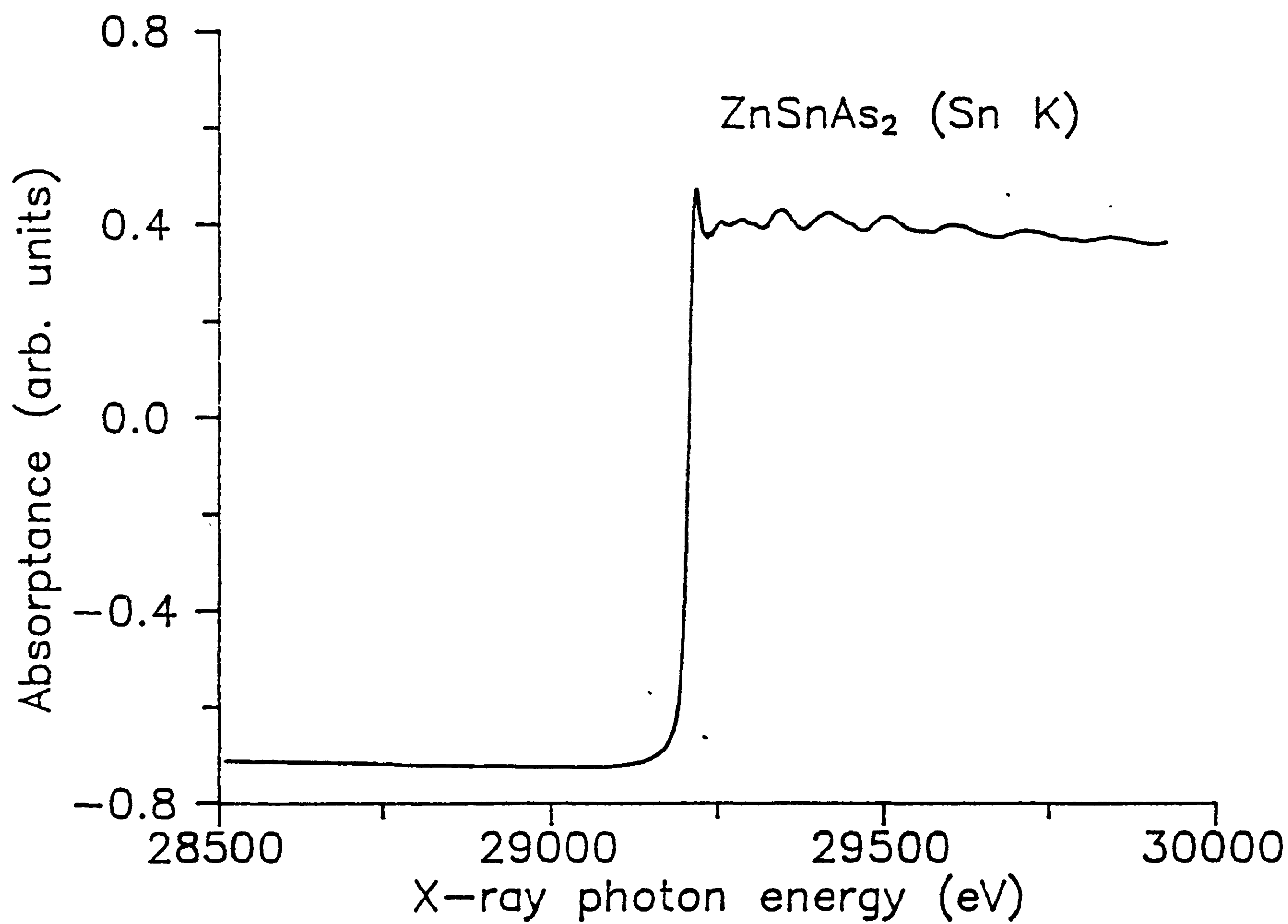

Figure 7. Sn K-edge absorptance of $ZnSnAs_2$ as function of x-ray photon energy.

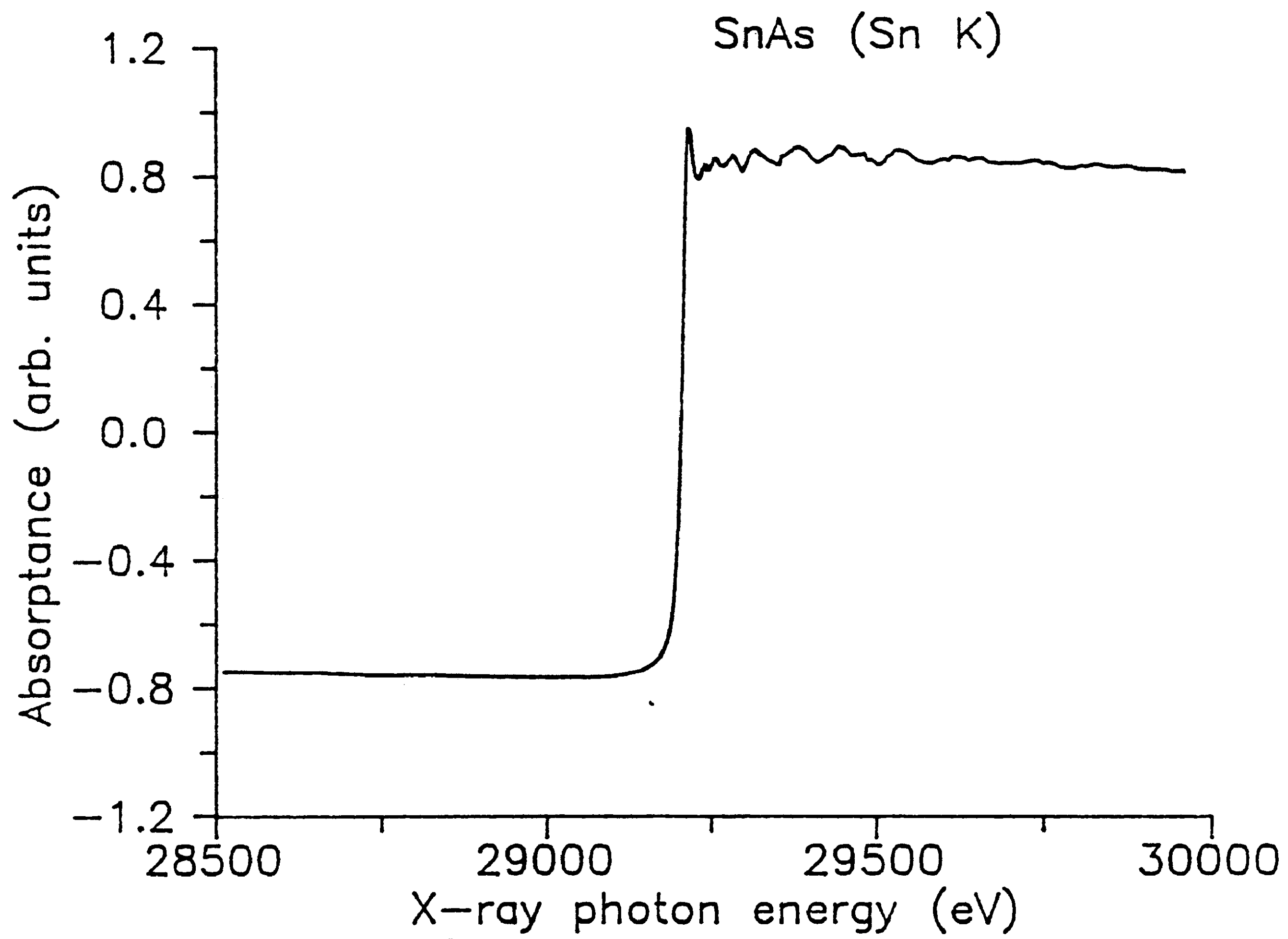

Figure 8. Sn K-edge absorptance of SnAs as function of x-ray photon energy.

EXPERIMENTAL TECHNIQUE

An EXAFS spectrum can be acquired by measuring the transmission of x rays, or the by-products of absorption. Fluorescence-detection EXAFS, discussed in detail below, is used widely. Other indirect techniques such as Auger electron yield or the total electron yield are also used. These various techniques differ in their detection schemes and in their suitability for different samples. The fluorescence-detection mode is used particularly to characterize dilute samples, and it was adopted to acquire Sn K-edge EXAFS data for the Sn-doped $Ga_{1-x}Al_xAs$ samples under investigation here. The transmission mode was used to acquire data for the two standards, $ZnSnAs_2$ and SnAs.

The experiments were carried out at beam line VII-3 of the electron storage ring (SPEAR) at the Stanford Synchrotron Radiation Laboratory (SSRL), in Palo Alto, California. The experimental arrangement (described in detail below) is shown in figure 9. The x-ray beam leaves the SPEAR vacuum system, passes through a helium atmosphere to the entrance slit of the monochromator 17.5 m from the source (Troxel, 1985). The monochromatized beam then emerges inside the shielded experimental area (hutch) where the sample and the detectors are located.

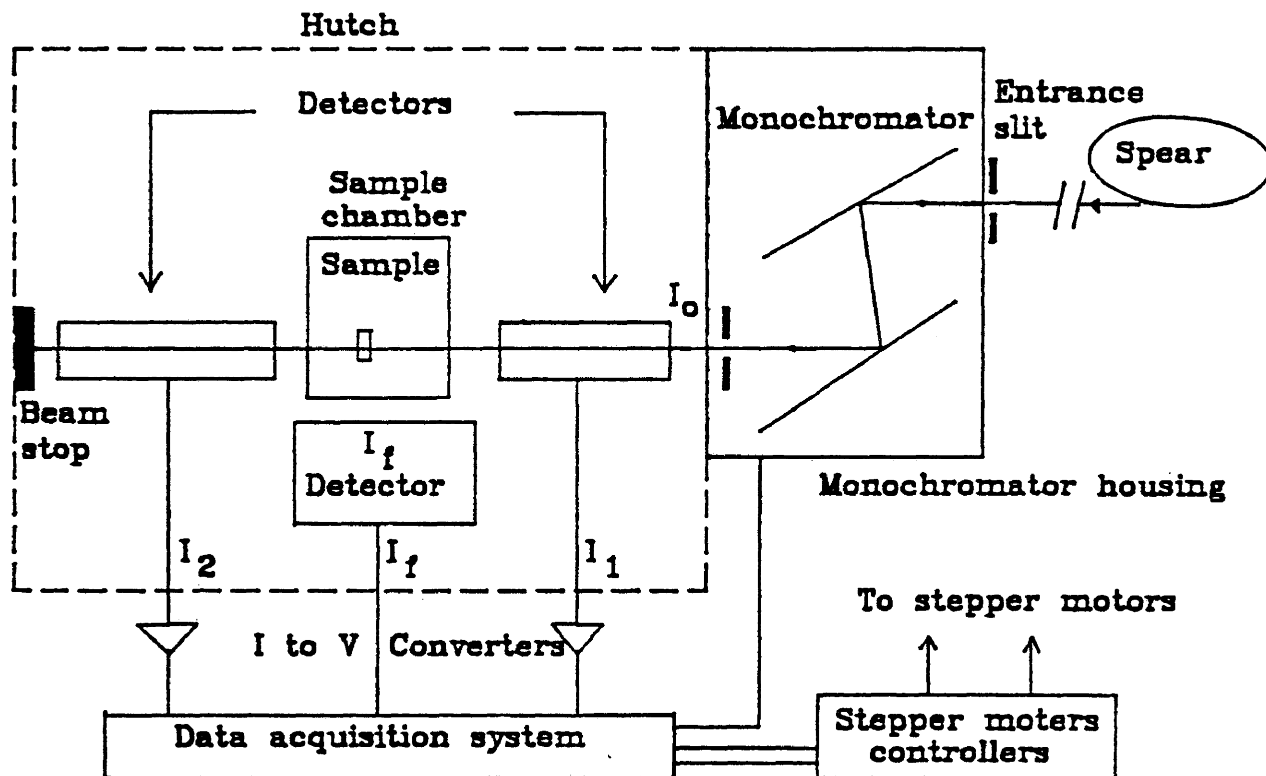

Figure 9. Experimental arrangement. The equipment is provided by SSRL (except for the sample chamber and the fluorescence detector).

X-ray source

Synchrotron radiation is produced by electrons traveling at relativistic velocities in a curved orbit. The radiation is emitted in a narrow cone centered about the direction of the velocity vector of the particles, and is linearly polarized for an observation point in the plane of the orbit (Hayes and Boyce, 1982). The intensity is on the order of 10^8 - 10^{10} photons/second in a 2 eV band width. Higher fluxes can be obtained by the use of wigglers. This last feature makes synchrotron radiation very attractive for EXAFS experiments where the absorptance or the fluoresence has to be measured with a good signal-to-noise ratio. During our experiments the energy of the stored electron beam was 3.0 GeV and the beam current ranged from 30 to 70 mA.

Monochromator

A Si(400) double crystal monochromator was used throughout the experiments. It enables variation of the energy of the incident x-ray photon around the edge of interest according to Bragg's law:

$$\hbar\omega = \frac{2\pi\hbar cn}{2d\ \sin\theta}$$

where n is the order of the reflection, d is the Bragg plane spacing and θ is the Bragg angle which is varied through a

stepping motor controlled by a PDP 11/34 computer. The various characteristics of the Si(400) monochromator are summarized in table 2 based upon the equations given in appendix A. The resolution of the monochromator is a function of the source size, the entrance slit width, and the x-ray energy. Poor resolution would result in distortion of the EXAFS spectrum, affecting the determination of the structural parameters (Hayes and Boyce, 1982).

One advantage of the double crystal monochromator is that the incident and the reflected x-ray beams are parallel as shown in figure 10. If the two crystals are separated by a distance D (typically 1 cm), the reflected beam is deflected vertically by an amount $2D\cos\theta$. As θ is scanned, the sample and the detectors are moved vertically to remain centered on the beam. Since the x rays then strike the sample at the same spot, problems due to sample nonuniformity are reduced.

One of the problems pertinent to the monochromator is the harmonic radiation which contaminates the exiting x-ray beam. These higher harmonics can interfere with the determination of the number of neighboring atoms (Hayes and Boyce, 1982). Higher-energy reflections, however, have narrower angular (or energy) widths than lower-energy ones, so that one can adjust (detune) the parallelism of the two crystals in a way that the second and higher harmonic

Table 2. Properties of the Si(400) double crystal monochromator.

d-spacing	: 1.358 Å
Band-width ($\Delta E/E$)	: $0.23\ 10^{-4}$
Crystal separation	: 10 mm
Energy range	: 2.8 to 50.0 KeV
Electron energy	: 3.0 GeV
Vertical source size	: 0.33 mm
Distance source-slits	: 17.5 m

	Monochromator slit size (mm)		
	0.5	1.0	2.0
Photon energy(eV)		Resolution (eV)	
28000	8.68	13.52	23.20
29000	9.29	14.49	24.88
30000	9.93	15.49	26.62

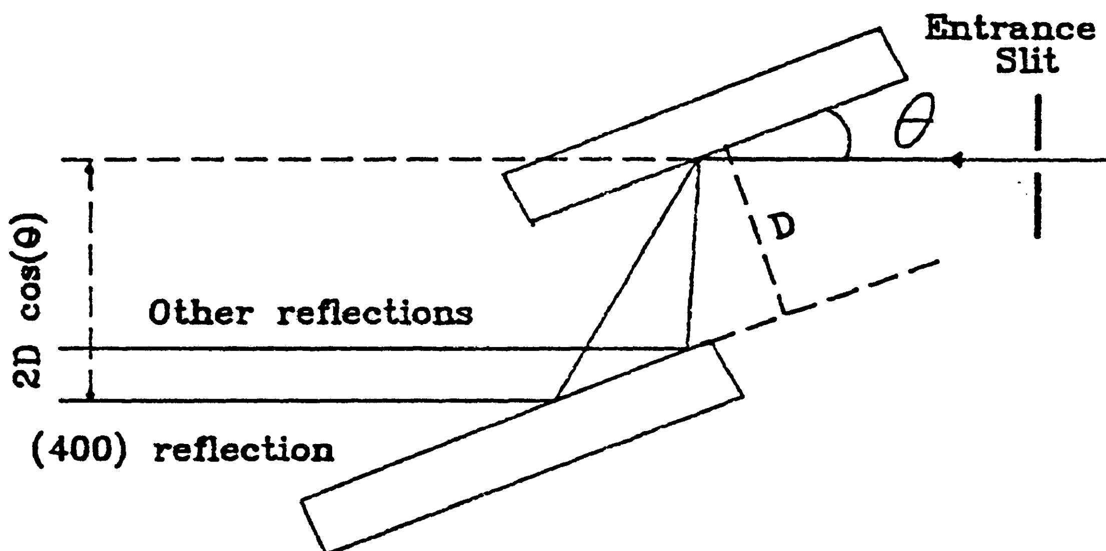

Figure 10. Schematic of the double crystal monochromator.

radiation not be diffracted by the second crystal of the monochromator. The detuning is carried out as follows: the piezovoltage controlling the parallelism is varied till the maximum in the incident intensity (I_1) is reached, then it is increased to the value corresponding to 75% of the maximum intensity. This procedure is repeated for each scan. The use of detectors with energy selectivity could also eliminate the problem with harmonics.

Detectors

The acquisition of an EXAFS spectrum requires the measurement of the intensity of the incident x-ray beam (I_1) and the transmitted intensity (I_2) for transmission experiments, or the fluorescent intensity (I_f) in the fluorescence mode. The three detectors used throughout the experiments are gas ionization chambers. Basically, an ionization chamber is a gas-filled capacitor. When the x-ray photons are absorbed, electron-ion pairs are created. The electric field between the electrodes sweeps the electrons away before they recombine with ions. This produces an electric current in an external circuit, which is converted to voltage, digitized and stored in the computer.

a. Transmission

The experimental arrangement for the detectors is shown

in figure 11. The first ion chamber, of length 15.2 cm monitors the intensity of the incident beam. The intensity measured is then given by

$$I_1=I_0[1-\exp(-\mu_1 l_1)] ,$$

where μ_1 and l_1 are, respectively, the absorption coefficients of the gas and the length of the ionization chamber, and I_0 is the incident intensity. The intensity of the beam is attenuated by $\exp(-\mu_1 l_1)$ as a result of traversing the first ionization chamber. Then it is attenuated by a factor of $\exp(-\mu_s z_s)$ passing through the sample, before it is monitored by the second ion chamber of length l_2 = 30.15 cm and absorption coefficient μ_2, which records an intensity given by

$$I_2 = I_0 \exp(-\mu_s z_s - \mu_1 l_1) [1 - \exp(-\mu_2 l_2)] ,$$

and thus

$$\mathrm{Log}(I_1/I_2) = \mu_s z_s + \mathrm{Log}\left[\frac{\exp(\mu_1 l_1) - 1}{1 - \exp(\mu_2 l_2)}\right] .$$

Since the absorption coefficients of the gases used in the detectors are smooth functions of energy, they contribute to the absorptance of the sample only a smoothly varying background which can be eliminated in the data analysis (see Data Analysis section). In order to maximize the signal-to-noise ratio (S/N), the thickness of the sample,

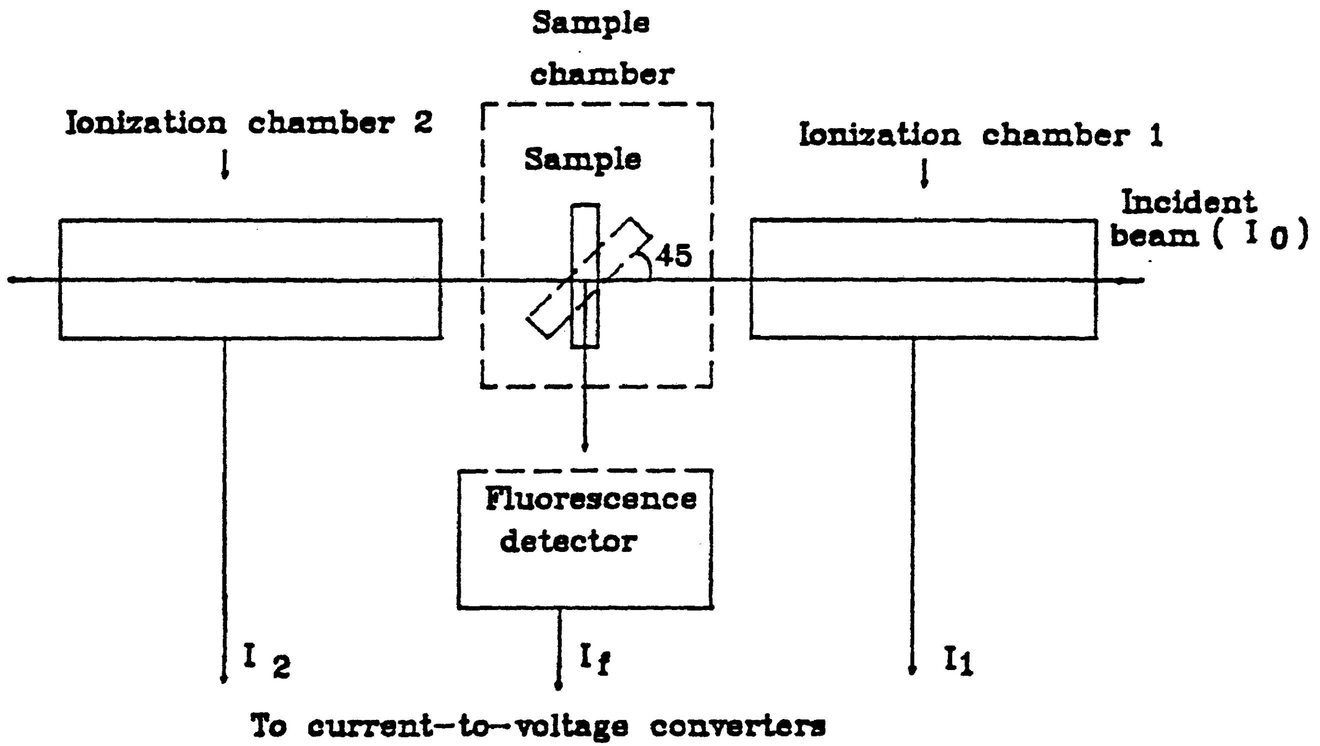

Figure 11. Arrangement of the detectors for a transmission/ fluoresence EXAFS experiments.

the length and the gas of the first ionization chamber should be such that: $\mu_s z_s = 2.55$ and $\mu_1 l_1 = 0.24$ at the absorption edge of interest (Hayes and Boyce, 1982). Argon was used in both ionization chambers. The mass absorption coefficient of Ar (μ/ρ where μ is the absorption coefficient and ρ is the density) is equal to 2.7 cm^2/g at 29200 eV. The absorption coefficient of our $Ga_{1-x}Al_xAs$ at a given energy can be estimated from tabulated mass absorption coefficients of Ga, Al and As, and can be used to calculate the thickness of the sample from the experimental absorptance (see appendix B).

b. Fluorescence

The underlying principle of the fluorescence-detection EXAFS is as follows. Upon photoexcitation of the core electron, a higher-lying electron fills the created hole with emission of a photon of characteristic energy

$$\hbar\omega_f = \Delta E \quad ,$$

where ΔE is the difference between the two energy levels. The fluorescence intensity is proportional to the probability that the incident radiation creates holes, and thus to the absorption rate. Therefore it will exhibit oscillations which correspond directly with those in the absorption coefficient (see Hayes and Boyce, 1982, for

details).

In the fluorescence detection mode, the sample and the detector are positioned at 45 and 90 degrees, respectively, relative to the incident beam (in the horizontal plane) to minimize the contribution of both elastically and inelastically scattered radiation to the background (Hayes and Boyce, 1982). The fluorescence signal was recorded using an ionization chamber equipped with a current to voltage converter and an amplifier, which provides a gain of 10^{10} to 10^{13} V/amp. This highly sensitive detector was made at the Colorado School of Mines (Small, 1989). Krypton was used as the detecting gas because of its relatively short absorption length. The absorption coefficient of Kr at the Sn K_{α} line (25.3 KeV) is 29.0 cm^2/g compared with 4.0 cm^2/g for Ar. This ensures that most of the fluorescence signal is detected. A silver filter, 100 μm in thickness, was used to filter the fluorescence signal for all the samples at the Sn K-shell absorption edge. These filters reduce the background signal resulting from inelastic and Compton scattered radiations and unwanted fluorescence from the sample and the substrate. The mass absorption coefficient of silver at 25.3 KeV is 8.88 cm^2/g and jumps to 50.4 cm^2 at 26.4 Kev. Generally, in fluorescence EXAFS, one uses filters having absorption edges between $\hbar\omega_f$ and the lower limit of the x-ray excitation energies of interest. Söller-slit

assemblies were used to reduce the contribution of the fluorescence signal from the filters.

Data acquisition system

The experiment is controlled by a PDP 11/34 computer. Data collection, sample and detector positioning, and Bragg angle scanning are done by this system through various interfaces. The motion of the monochromator is controlled by a stepper motor. The experimental apparatus resides on a table the height of which is varied through another stepper motor. This permits the sample and the detection system to track the deflected beam as mentioned above.

Experimental procedure

Before taking data, one must align the samples and the detectors in the beam. This is done by taking successive pictures of the beam (using x-ray sensitive Polaroid film) at the entrance slit of the hutch, and at the entrance and exit windows of the dewar. Once the beam and the sample holder are aligned roughly by moving the table up and down, a Pb cross-hair is placed at the center of the sample holder and a fine adjustment is done until the cross-hair is exactly centered in the beam. It is also necessary to calibrate the monochromator with a sample of known absorption edge (Sn foil for example). The samples are

introduced into the dewar, and cooled to the desired temperature. The offsets, corresponding to the dark counts of the detectors, are measured, the monochromator crystal detuned, and the data collection program is started. The last two procedures are repeated for each scan. The data from each scan is stored on magnetic tape together with headers for identifying the sample and relevant parameters for later use in the data analysis.

Generally EXAFS spectra are contaminated by noise originating from different sources, such as the detectors and fluctuations in the incident intensity. This effect is pronounced in the fluorescence detection mode where the signal is very small due to the low concentration of the excited atoms. Therefore it is usually necessary to obtain a large number of spectra for each sample, which are added up later to increase the S/N ratio.

SAMPLES

Our goal is to probe the local environment of Sn impurities in GaAs and $Ga_{0.7}Al_{0.3}As$. The different Sn-doped $Ga_{1-x}Al_xAs$ samples are listed in table 3, which also shows the donor concentration, Hall carrier concentration at 300 K and 77 K. Carrier freeze-out is clearly manifest in the dramatic decrease in the carrier concentration when the temperature decreases.

These samples were grown by MOVPE in France on semi-insulating GaAs <100> substrates. Sn-doping was achieved using a $Sn(CH_3)_4$ source. The samples were characterized electrically by Hall measurement and photoluminescence (see Eljani et al., 1988, for preparation and characterization details).

The samples were subsequently prepared for EXAFS measurements by lapping to remove the GaAs substrate from each $Ga_{1-x}Al_xAs$ sample. This process fractured these brittle materials. The resulting flakes from each sample are carefully mounted in a graphite holder with bee's wax, forming approximately three layers.

To increase the fluorescence signal, a stack of two as-made samples was used for each measurement. For the ionized (shallow donor in GaAs) state, the sample made from EX1A was stacked on top of the one made of EX1B. For the

Table 3. Properties of $Ga_{1-x}Al_xAs$ EXAFS samples.

Sample code	x	Thickness (μm)	Nominal N_d (cm^{-3})	n_H (cm^{-3}) 300 K	77 K
EX1A	0.0	28	$5x10^{18}$	$3.8x10^{18}$	-
EX1B	0.0	20	$5x10^{18}$	$1.8x10^{18}$	$1.9x10^{18}$
EX3A	0.32	24	$5x10^{18}$	$2.2x10^{16}$	$1.2x10^{15}$
EX3B	0.27	29	$5x10^{18}$	10^{17}	$7.1x10^{15}$

supposedly relaxed Sn state (DX center), the sample made from EX3B was stacked on top of the one from EX3A. In each case, the top sample was facing the incident x rays and would therefore dominate the measured spectra.

Our procedure for extracting the structural parameters from the EXAFS measurements consists of comparing EXAFS data from the structurally unknown sample with standards. To this end, $ZnSnAs_2$ (chalcopyrite structure) and SnAs (sodium chloride structure) were used. The lattice parameters, nearest-neighbor distances (nnd), and coordination numbers are listed in table 4. The equations used to calculate the different nnd are listed in appendix C.

It is well known that the crystal structure of GaAs is zincblende. The doped samples were grown so that Sn atoms substitute for the Ga atoms, and therefore occupy tetrahedral group III sites. The structure of $Ga_{1-x}Al_xAs$ differs from that of GaAs by the fact that group III sites in the former are randomly occupied by Ga and Al atoms. The lattice constant changes from 5.652 Å for GaAs (x=0) to 5.662 for AlAs (x=1).

The sample chamber consists of a dewar which is cooled with liquid nitrogen. The samples are mounted on a probe with vacuum grease, then introduced into the dewar. One load can accommodate four samples. Each sample can be brought into vertical alignment with the beam using calibrated

Table 4. Lattice parameters for $ZnSnAs_2$, SnAs, and GaAs.

	a (Å)	c (Å)	nnd (Å)	Coordination number
$ZnSnAs_2$	5.85	11.70	2.60	4
SnAs	5.72		2.86	6
GaAs	5.65		2.45	4

spacers, thus eliminating the need to reload the chamber for each run. The sample holder was equipped with a thermocouple to monitor the temperature of the sample.

DATA ANALYSIS

Addition of the data sets

Our procedure for extracting structural information requires that the EXAFS data for the standards and the structurally unknown system be treated in exactly the same way during processing.

For each sample, the individual data sets are carefully examined. The sets containing spurious spikes or an unusually large amount of noise are discarded. The remaining data files are added up and either I_f/I_1 or $Log(I_1/I_2)$ is calculated, depending whether the data was collected in fluorescence or in transmission. This procedure increases the signal to noise (S/N) ratio by a factor of as much as $(n)^{1/2}$ where n is the number of files added up, assuming that the noise is statistical in origin.

A problem encountered during file addition is that the threshold energy (E_{th}) varies even among the data sets taken at different times for the same sample and for the same excited atom, due to the looseness of the mechanical parts involved in the motion of the monochromator or the movement of the x-ray beam. This is corrected as follows: E_{th} is determined for each file following the method described below; an average threshold energy is then found. The data file having a threshold energy closest to the average is

taken as reference. The other spectra are then shifted by an amount E_{th}(reference)-E_{th} using linear interpolation before they are added to the reference. One also takes into account the differences in integration time of each data point and in the gains of the amplifiers used for the data sets.

Extraction of the EXAFS signal

The first step in the analysis of EXAFS data is to isolate $\chi_\alpha(\omega)$ from the absorption coefficient data or from the ratio I_f/I_1. There are two contributions to the experimental absorption of the sample: the first is from the Sn K-shell (μ_{Sn}), which contains the EXAFS of interest; the second is a slowly varying background absorption (μ_{bg}). The procedure described below is based upon the equation (Hayes and Boyce, 1982),

$$\chi_\alpha(\omega) = \frac{\mu_s(\omega) - [\mu_\alpha{}^0(\omega) + \mu_{bg}(\omega)]}{\mu_\alpha{}^0(\omega)} .$$

First, the threshold energy (E_{th}) is determined by extrapolating the absorption from below and above the edge (excluding the contribution from the threshold feature). The intersection of the average of these two curves with the edge step corresponds to E_{th}, and the difference between the two fitted curves at E_{th} is the edge height, which is

directly proportional to the number of excited atoms. The fits are done using a linear combination of Chebyshev polynomials. The orders of the pre-edge, post-edge and edge fits were always set equal to three (i.e., quadratic in E) to exclude the rapidly varying oscillations during the fits. Chebyshev polynomials were used because they are orthogonal to one another and can be calculated recursively which makes the normal equation easy to compute (second degree cubic splines could also be used for this purpose). This procedure was used for the different data files of the samples under investigation.

The background signal μ_{bg} and the free atom absorption coefficient $\mu_{\alpha}{}^{0}$ are both extracted by fitting the EXAFS region, which extends from just above the threshold feature to upper limit of the data range, with a linear combination of Chebyshev polynomials in $(\hbar\omega-E_{th})^{1/2}$. The coefficients of the expansion are found by at least-squares fitting method wherein the deviations are weighted by $(\hbar\omega-E_{th})$. This weight is introduced to improve the fit at high values of electron energy. The resulting curve is subtracted from the absorptance. The yield is then normalized with respect to the edge height. This procedure will normalize the EXAFS signal to a per-atom contribution and thus allow comparison between samples. The normalization results in the EXAFS signal $\chi_{\alpha}(\omega)$ as a function of the energy of the incident

photons. The next step is to obtain χ in terms of the photoelectron wave number k. To this end, one needs to find a one to one relationship between k and $\hbar\omega$. These two variables are related through the equation derived from the conservation of energy,

$$k = \sqrt{\frac{2m}{\hbar^2}\left(\hbar\omega - (E_0 - E_{1s})\right)}$$

Therefore one needs an accurate evaluation of E_0-E_{1s} which is not possible in practice due the absence of an explicit and accurate representation of the interaction of the photoelectron with the rest of the electrons. E_0-E_{1s} differs from the threshold for the continuum excitation (E_{th}) by the Fermi energy and a self-energy term (Hayes and Boyce, 1982). Since our analysis involves only comparisons between data sets, the threshold energy E_{th} is assumed to coincide with E_0-E_{1s} for all the samples. This distorts all data sets similarly and would not affect our conclusions if there were not chemical shifts in E_0-E_{1s} from one material to another. To compensate for this, we treat E_{th} as a parameter in the data analysis. The validity of this procedure is supported by the small shifts needed in E_{th} (typically a few eV).

Figures 12 and 13 show the as-extracted $k\chi$ signal from the previously shown $ZnSnAs_2$ and SnAs absorptances as a function of the photoelectron momentum k. The parameters used are listed in table 6. The pre-edge and post-edge fits are used to find the threshold energy. The final fit is carried out to extract the background from the data. The feature around 2 $Å^{-1}$ corresponds to the white line at threshold. The presence of at least two frequencies indicates a contribution from at least two shells of neighbors around the Sn atoms in both cases. We also note that the fundamental frequency is higher in SnAs, as expected since the nnd is larger in this case (2.86 Å vs 2.6 Å). Qualitative information can be inferred from the comparison of two EXAFS spectra in k-space but for quantitative results we need to isolate the contribution of each coordination shell by Fourier transformation of the $k\chi$ signal into r-space.

Fourier Transformation

Generally the $k\chi(k)$ data contains contributions from many shells around the absorbing atoms so that extraction of structural parameters in k-space before Fourier filtering is difficult. Being the Fourier transform (FT) of an extended function in k-space, the FT of the EXAFS signal will be localized in r-space. This enables separation of the

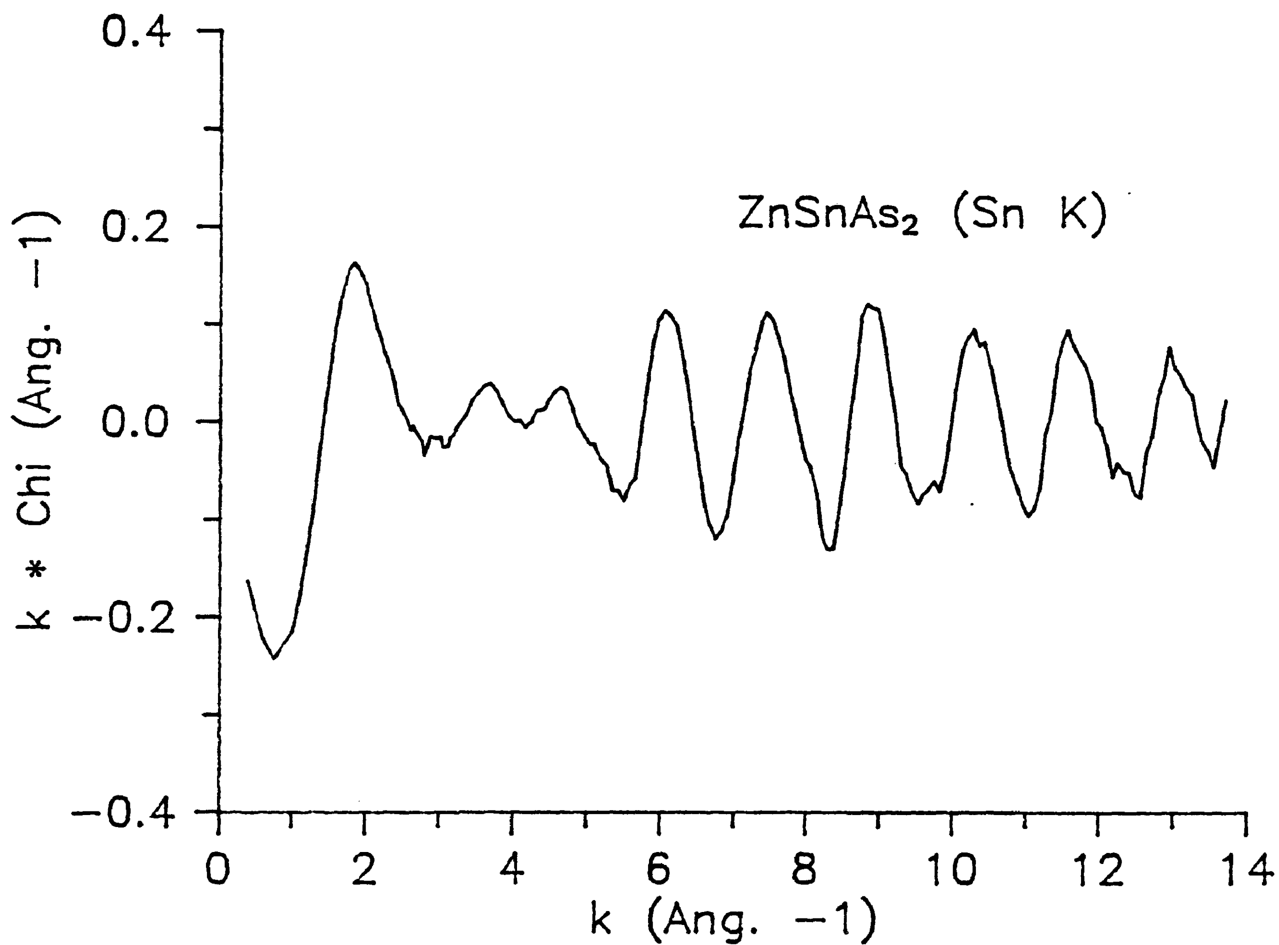

Figure 12. EXAFS oscillations $k\chi(k)$ on the Sn K-shell absorptance of $ZnSnAs_2$ as a function of the photoelectron momentum k.

ARTHUR LAKES LIBRARY
COLORADO SCHOOL of MINES
GOLDEN, COLORADO 80401

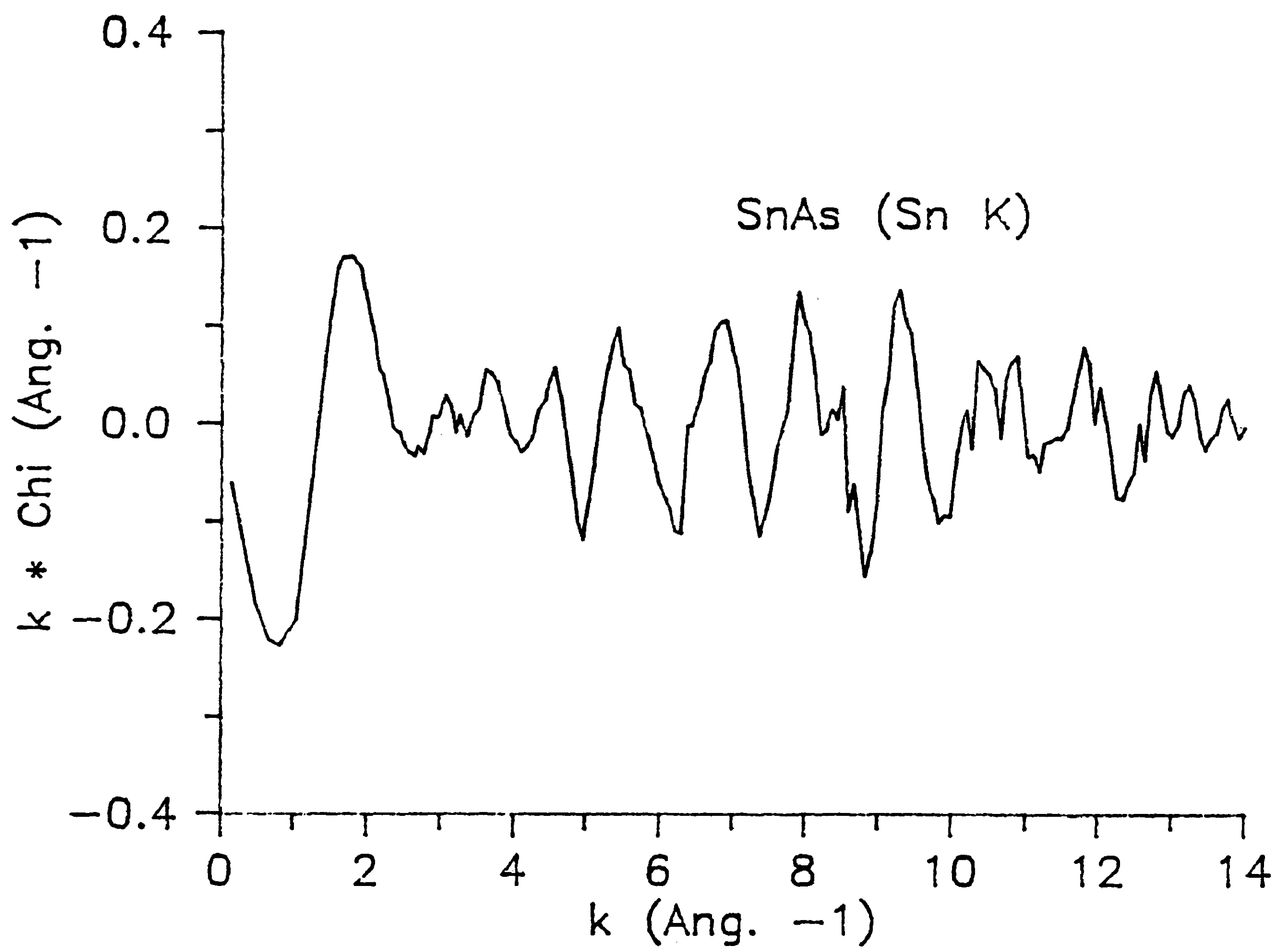

Figure 13. EXAFS oscillations $k\chi(k)$ on the Sn K-shell absorptance of SnAs as a function of the photoelectron momentum k.

Table 5. Parameters used to extract $k\chi$ from the $ZnSnAs_2$ and SnAs absorptances.

	Energy Ranges (eV)	
	$ZnSnAs_2$	SnAs
Pre-edge fit	28344.0 - 29098.11	28344.0 - 29066.88
Post-edge fit	29211.07 - 29921.03	29211.82 - 29953.14
Edge fit	29196.53 - 29208.65	29197.00 - 29206.80
Final fit	29223.18 - 29921.03	29221.71 - 29953.14
Order of final fit	7	7
Edge energy (eV)	29203.44	29203.16
Edge height	1.133	1.6167
Window for FT ($Å^{-1}$)	2.67 - 12.81	2.67 - 12.81
σ for FT ($Å^{-1}$)	0.5	0.5

contributions from different shells around the central atom in r-space. The FT of $k\chi$ is given by (Hayes and Boyce, 1982):

$$\phi(r) = \frac{1}{(2\pi)^{1/2}} \int_0^\infty W(k)\ k\chi(k)\ \exp(-2ikr)d(2k)\ .$$

The window W(k) is necessary because of the finite experimental range of the data which imposes an upper limit on k (k_{max}). A lower limit on k (k_{min}) is imposed by the fact that multiple-atom scattering effects predominate at lower k and thus the single scattering formula for χ is no longer valid. If an explicit window function is not used there will be an effective square window defined by k_{min} and k_{max}, the FT of which is proportional to $\sin(r\Delta k)/(r\Delta k)$, where $\Delta k = k_{max}-k_{min}$. This function has a long-range oscillatory nature which transforms any sharp features in the experimental $\phi(r)$ into oscillatory functions. This causes interference between near neighbor peaks and hinders the extraction of structural parameters (see Hayes et al., 1976, for a detailed discussion). To avoid this problem, a Gaussian-broadened square window was used, which results in an exponential localization of the peaks in $\phi(r)$ (Hayes et al., 1976), thus lessening the interference between the near neighbor peaks. All the data were transformed using a square window between 2.67 and 12.81 $Å^{-1}$, broadened by convolution

with a Gaussian of halfwidth 0.5 $Å^{-1}$. The lower limit of the window avoids the threshold peak. The upper limit avoids the large noise in the EXAFS at high k, especially for dilute samples.

The FT's for the $ZnSnAs_2$ and SnAs data are shown in figure 14 and 15, respectively. The solid line represents the real part of $\phi(r)$ and the dashed line represents its magnitude. The large peak corresponds to the signal from the four As ($ZnSnAs_2$) or the six As (SnAs) nearest neighbors around the Sn central atom. The position of this peak does not correspond exactly to the nn distance because of the linear term in the phase shift (due to the potential of the central and the backscattering atoms) and the choice of E_0. The shift depends also on the width of the window used for the FT. The peaks above 3 Å contain contributions from the second and higher coordination shells. The ones below 1.5 Å are due to the incomplete removal of the background signal from the EXAFS data. The latter effect can be reduced by increasing the order of the final fit in the previous step, but eventually at the expense of a decrease in the amplitude of the EXAFS.

Extraction of structural information

The method used throughout this work was first introduced and applied by Hayes et al. (1976). It is based

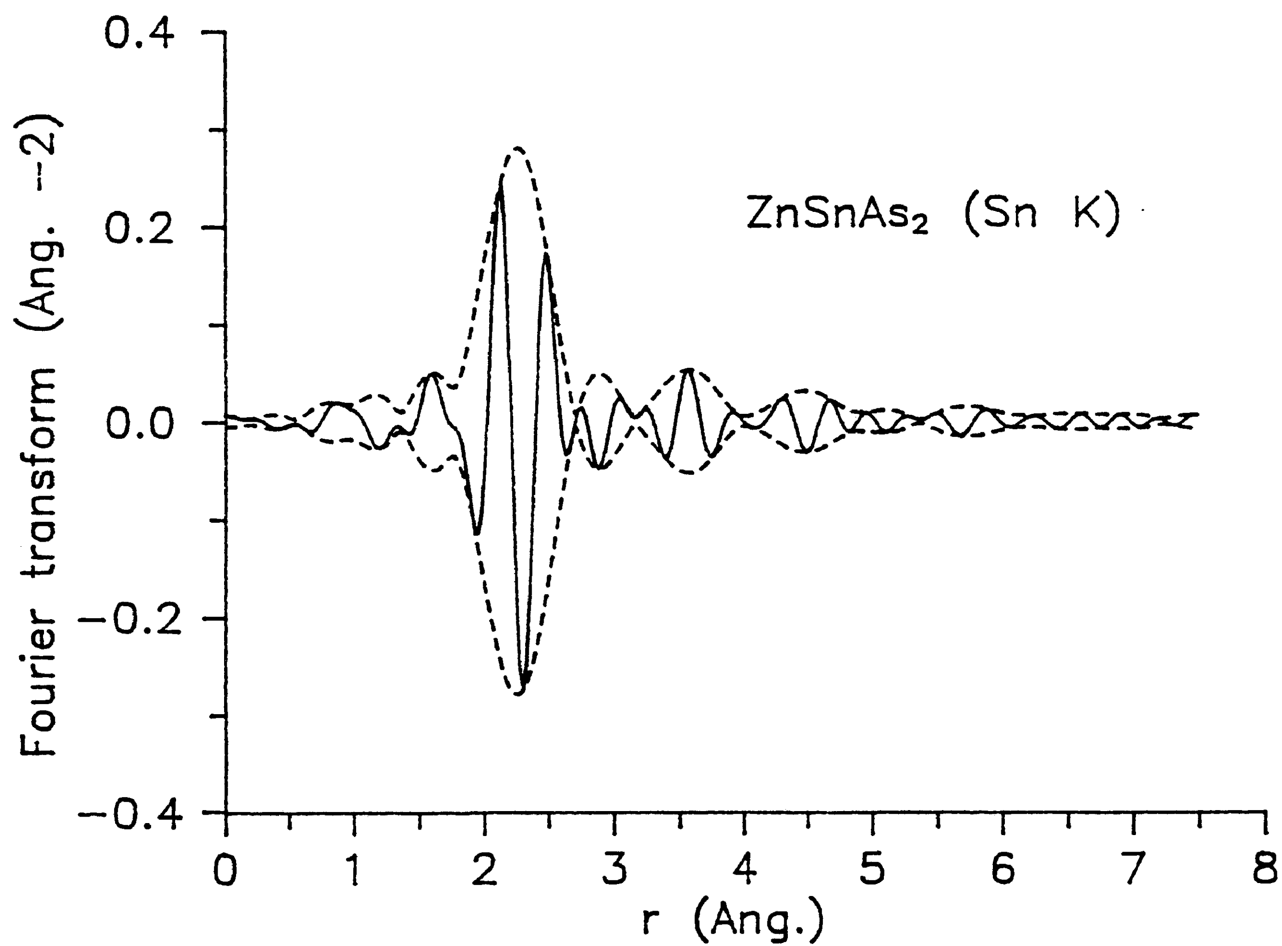

Figure 14. Magnitude (dashed lines) and real part (solid line) of the Fourier transform of $ZnSnAs_2$ $k\chi(k)$ obtained using a (2.67,12.81) $Å^{-1}$ square window broadened by a Gaussian of halfwidth 0.5 $Å^{-1}$.

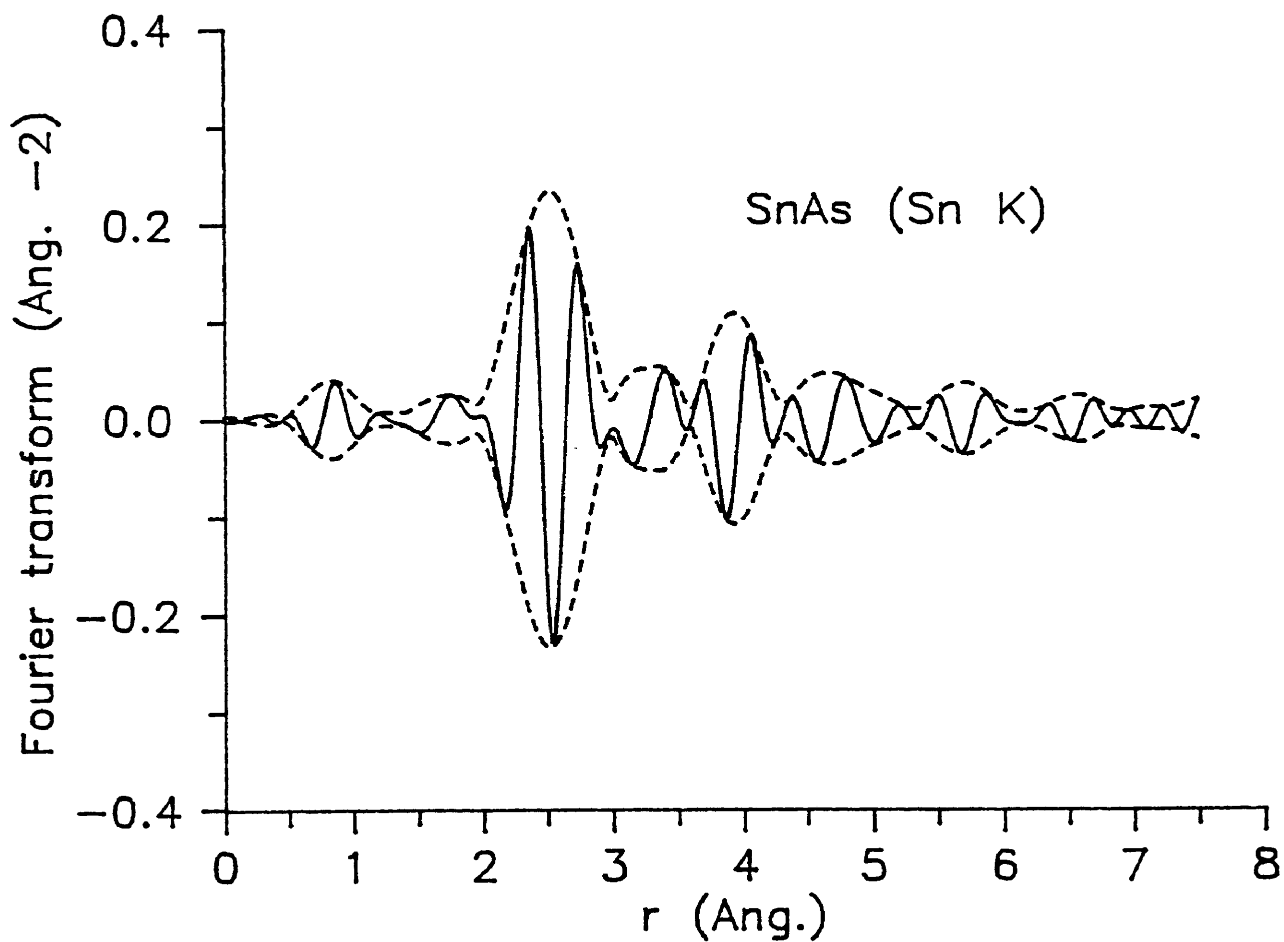

Figure 15. Magnitude (dashed lines) and real part (solid line) of the Fourier transform of SnAs $k\chi(k)$ obtained using a (2.67,12.81) $Å^{-1}$ square window broadened by a Gaussian of halfwidth 0.5 $Å^{-1}$.

on the following argument. From the expression of $\phi(r)$,

$$\phi(r) \simeq \sum_{\beta} \left[\frac{p_{\alpha\beta}(r)}{r^2} \right] * \xi_{\alpha\beta}(r) \quad ,$$

it can be seen that each contribution is given by the convolution of a peak function $\xi_{\alpha\beta}$ centered near r=0 and a radial distribution function $p_{\alpha\beta}(r)$. For sharply peaked pair distributions, $\phi(r)$ is basically a linear combination of the peak functions. This property is exploited as follows. The peak function $\xi_{\alpha\beta}$ is extracted from a standard. A model $\phi_m(r)$ for the structurally unknown system can be calculated using the extracted peak function with appropriate shifts in position and amplitude, and broadened by convolution with a Gaussian distribution. The model parameters are the nnd, the relative coordination number and the Gaussian half-width. They are varied until the best fit to the measured $\phi(r)$ is reached, corresponding to a minimum of the residual error R given below:

$$R^2 = \frac{1}{2N} \sum^{N} \left[\frac{[\mathrm{Re}(\phi - \phi_m)]^2}{(\mathrm{Re}\phi)^2 + (\mathrm{Re}\ d\phi/dr)^2} + \frac{[\mathrm{Im}(\phi - \phi_m)]^2}{(\mathrm{Im}\phi)^2 + (\mathrm{Im}\ d\phi/dr)^2} \right]$$

where N is the number of points in the range of comparison (Hayes and Boyce, 1982). The derivatives are introduced into the expression for R to enhance its sensitivity to variations in the peak shape at the expense of sensitivity

to position. The range of comparison is chosen to focus on one peak in $\phi(r)$. To this end, the amplitude of the peak to be fit is measured, and then the intersections of the magnitude of $\phi(r)$ with the line corresponding to 1/4 of that amplitude are taken as the window limits.

This analysis requires that the absorbing and the scattering atoms are the same in the standard and the structurally unknown system, and that the data are transformed from k to r using the same window. It also assumes the chemical transferability of the phases in $\Lambda_{\alpha\beta}$. This amounts to the requirement that $\Lambda_{\alpha\beta}$ varies little between the standard and the structurally unknown system. The method described above yields the relative amplitude, from which the coordination number can be found given that of the standard, the r-shift (Δr) corresponding to the difference between the nn distances, and the relative broadening ($\Delta\sigma^2 = \sigma^2{}_s - \sigma^2{}_{std}$, where σ_s and σ_{std} are the half widths of the pair distribution of the sample and the standard respectively). Note that $\Delta\sigma^2$ can be positive or negative depending on the relative widths of the two peaks being compared.

This procedure was used to extract the structural parameters for $ZnSnAs_2$ using SnAs as a standard and vice versa. The position of the first nearest neighbor for the standard was set equal to the value calculated from the

lattice parameters. The edge energy was shifted to minimize the residual error R as mentioned above. The results corresponding to the minimum in R for $ZnSnAs_2$ and SnAs are shown in table 7. These results demonstrate clearly that the first nn peak of Sn in SnAs is broader. The difference in experimental nn distances is in good agreement with the calculated one. Note that the calculated nn distance in $ZnSnAs_2$ takes into account the As displacement from its ideal position as proposed by Jaffe and Zunger (1984). When this displacement is ignored, the calculated nnd is found to be 2.53 Å, which is 0.09 Å different from the experimental nnd. The quality of the fits, which is given by the residual error R, is excellent in both cases.

Table 6. Structural Parameters of $ZnSnAs_2$ and SnAs.

	$ZnSnAs_2$	SnAs
Standard	SnAs	$ZnSnAs_2$
Range of fit (Å)	1.88 - 2.6	2.08 - 2.88
Δr (Å)	-0.244	0.246
Relative amplitude	0.666	1.5
$\sigma^2{}_s - \sigma^2{}_{std}$ (Å^2)	-0.0014	0.0024
R minimum	0.0054	0.012
E_0(std)-E_0(s) (eV)	+2	-1
Experimental nnd (Å)	2.62	2.85
Calculated nnd (Å)	2.60	2.86
Coordination number	4	6

RESULTS AND DISCUSSION

EXAFS Results for Shallow Sn Donors in GaAs

24 scans were performed for this sample (described above). Only 14 of them were judged suitable to be added together following the considerations discussed above. The resulting I_f/I_1 spectrum is presented in figure 16. The background in the I_f/I_1 ratio increases with incident photon energy because the transmission of the background radiation by the Ag filter increases with photon energy. We note that the threshold energy of the added data sets varied from 29203.5 to 29210.4 eV. The possible causes of this effect were discussed earlier.

Extraction of the EXAFS $k\chi$, shown in figure 17, followed the method described in the last section. The parameters used for this purpose are listed in table 7. We note that the final fit used to remove the background signal is of order 9. Attempts to use fits of order 7 or 8 were made but the standard deviations of the fits were too large, resulting in curves which did not follow the background signal. The Fourier transform $\phi(r)$ of the EXAFS is shown in figure 18. Comparing the nearest-neighbor peaks in GaAs and $ZnSnAs_2$ (at $\sim$2.2 Å), it can be seen that their amplitude and real part (related to the phase) are similar. This is a qualitative indication that Sn atoms have similar nn

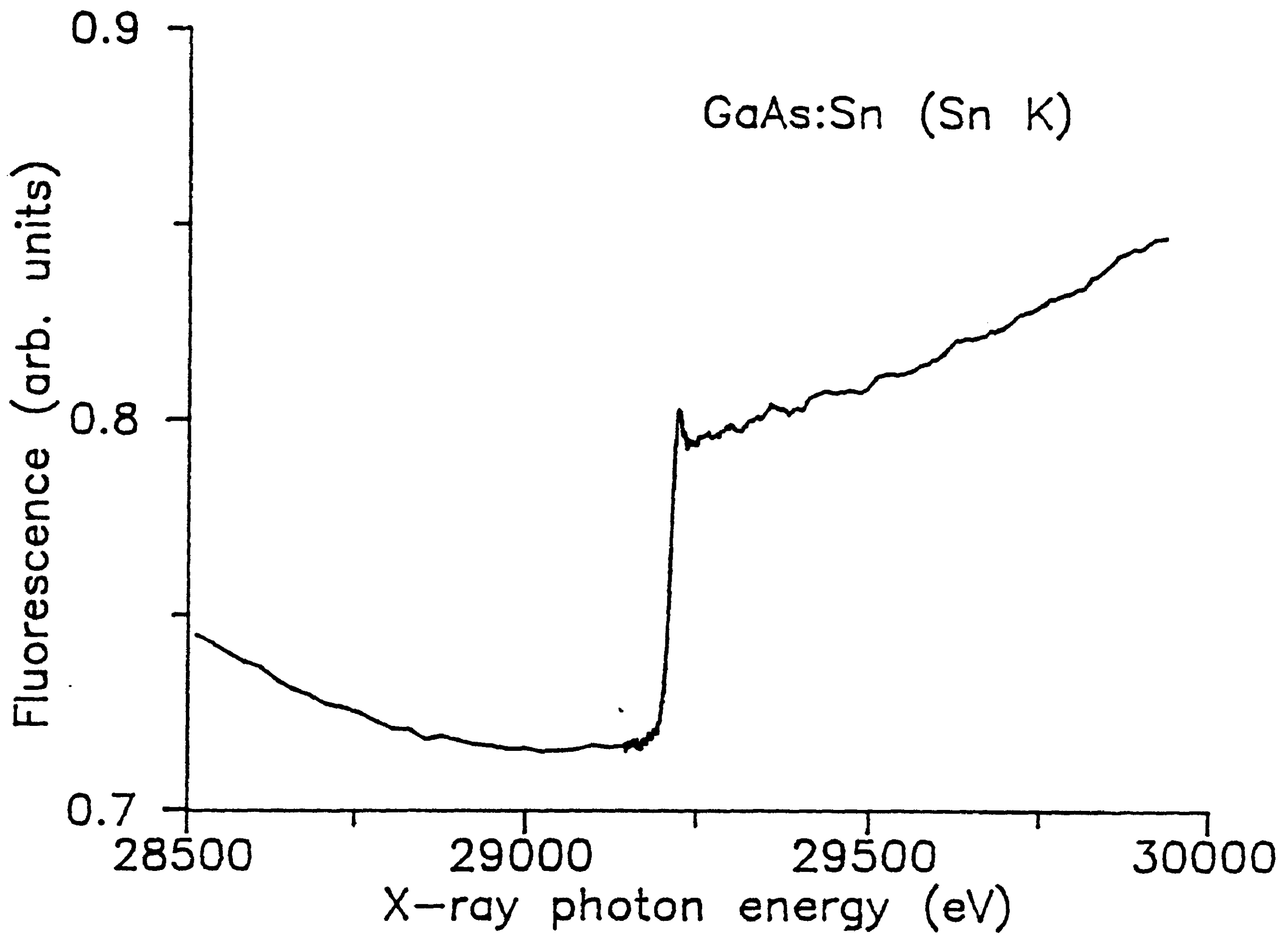

Figure 16. Sn K-shell fluorescence yield of GaAs:Sn as function of incident photon energy.

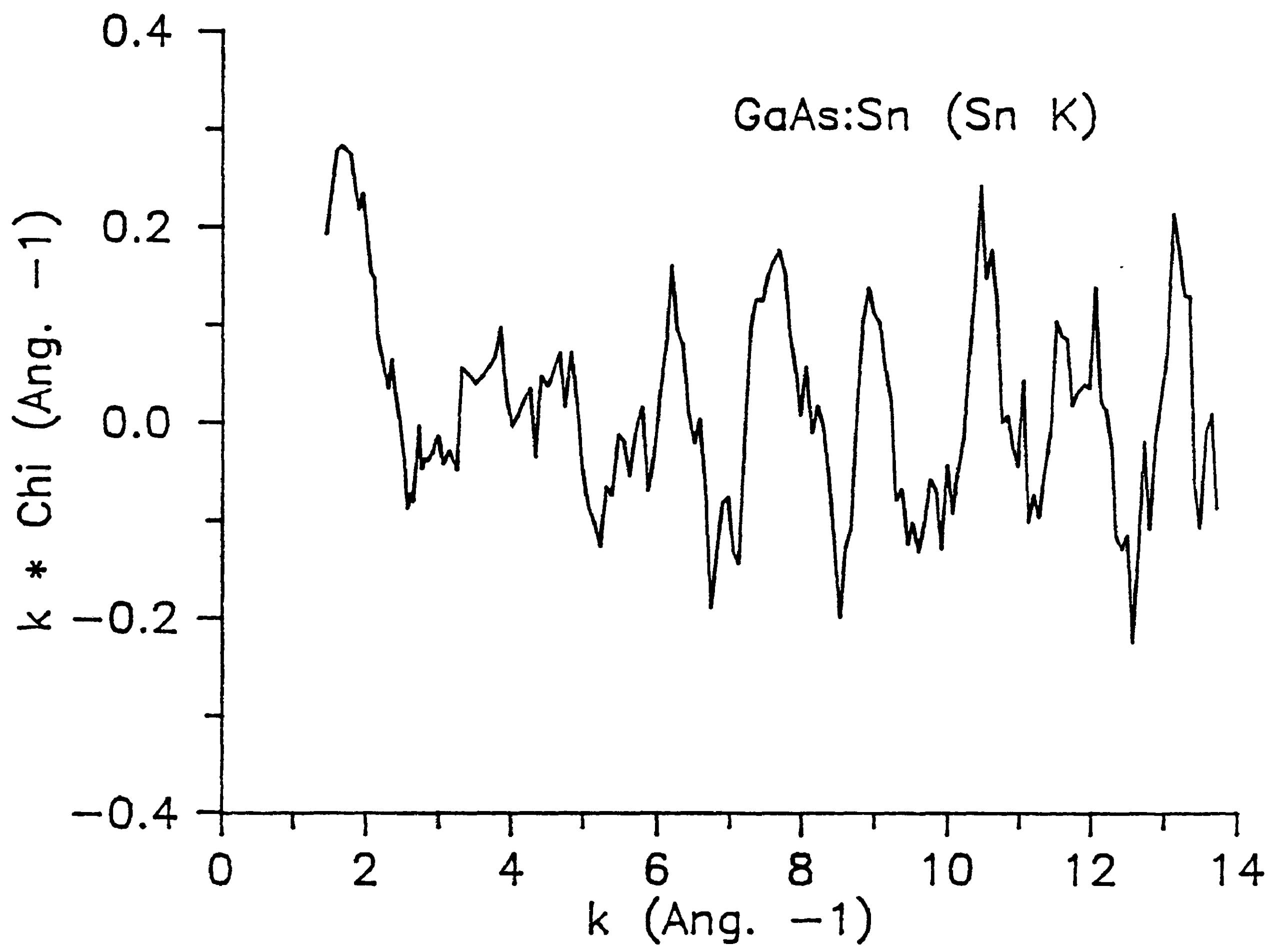

Figure 17. EXAFS oscillations $k\chi(k)$ on the Sn K-shell fluorescence of GaAs:Sn as function of the photoelectron momentum k.

Table 7. Parameters used to extract $k\chi$ from GaAs:Sn data.

	Energy ranges
Experimental range	28368.52 - 29931.91
Pre-edge fit	28368.52 - 29137.88
Post-edge fit	29215.82 - 29927.04
Edge fit	29203.64 - 29210.95
Final fit	29225.70 - 29929.48
Order final fit	9
Edge energy (eV)	29208.2
Edge height	0.077
Window for FT ($Å^{-1}$)	2.67 - 12.81
σ for FT ($Å^{-1}$)	0.5

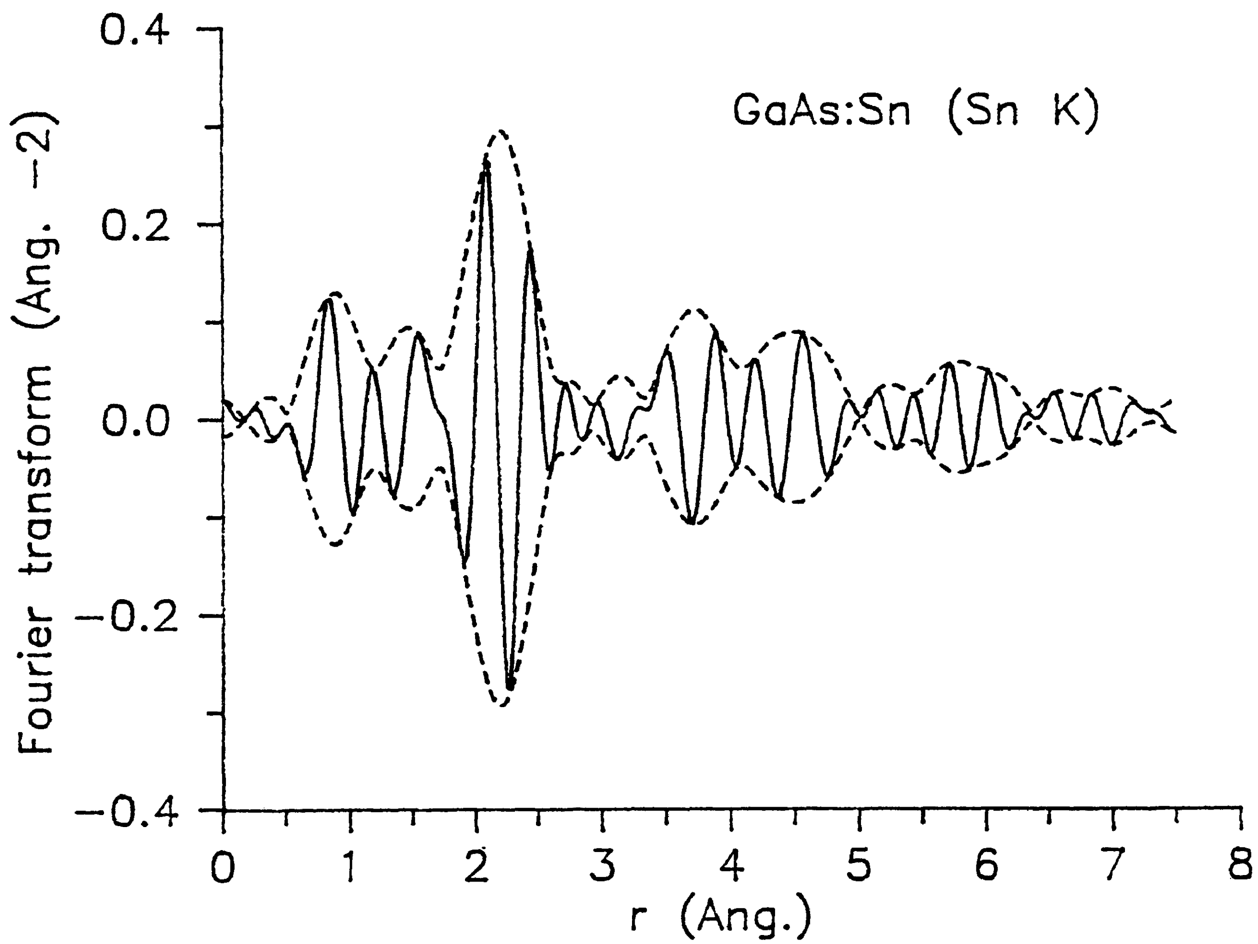

Figure 18. Magnitude (dashed lines) and real part (solid line) of the Fourier transform of GaAs:Sn $k\chi$ obtained by using a (2.67,12.81) $Å^{-1}$ square window broadened by a Gaussian of halfwidth 0.5 $Å^{-1}$.

environments in the two samples.

The peak function, ξ_{Sn-As}, extracted from the FT of the $ZnSnAs_2$ data was used to fit the nn peak for this sample because the Sn atoms have presumably the same nearest-neighbor environment in both materials (tetrahedral coordination with As). The range of the fit was 1.8 - 2.56 Å. The relative amplitude of the peak was fixed at one, corresponding to 4 As neighbors. These fits yielded Δr = -0.039 Å with a residual error R = 0.026. Subsequently, the threshold energy of GaAs:Sn was shifted in steps of 0.5 eV in order to reach a minimum in the residual error. This minimum occurs at ΔE_0 = -3.5 eV with the following results: Δr = -0.050 Å and R = 0.015 (see table 8). We note that shifting the edge energy improved the quality of the fit considerably. When the constant amplitude restriction is removed, the radial shifts and the width of the peak change only slightly. The relative amplitude of the peak was found to be 1.0 ± 0.1 for the best fits, suggesting that the coordination number is four. These fits also revealed that the nn peak in GaAs is narrower than the nn peak of the standard.

The above fits assume that the difference between the nn peaks in the standard and the structurally unknown sample (referred to hereafter as the peak shape) can be represented by convolution with a Gaussian. Two-peak fits using a

Table 8. Structural parameters of Sn in GaAs.

Standard : $ZnSnAs_2$

Range of comparison : 1.8 - 2.56 Å

One-peak fits

ΔE_0 (eV)	Amplitude	Δr (Å)	$\Delta\sigma^2$ (Å^2)	R
0.0	1.0	-0.039	-0.0004	0.026
-3.5	1.0	-0.050	-0.0004	0.015

Two-peak fits

ΔE_0 (eV)	Amplitude	Δr (Å)	$\Delta\sigma^2$ (Å^2)	R
-0.5	0.75	-0.003	-0.002	0.009
	0.25	-0.100	-0.005	
-0.5	0.5	0.024	-0.003	0.009
	0.5	-0.097	-0.004	

$ZnSnAs_2$ signature were also carried out in order to detect any deviation from a Gaussian peak shape. The results of these fits are presented in table 8. Note that the sum of the amplitudes of the two peaks is fixed at 1, corresponding to four As neighbors. The minimum residual error R is $\sim$0.009, and occurs at ΔE_0 = -0.5 eV. Note first that the deduced positions of the two peaks are so close in both cases that the result is more properly regarded as a single asymmetric nn distribution than as two distinct nn distances or as two distinct environments. Secondly, the small shifts in the edge energy and the low value of R lead us to the conclusion these last fits best represent the Sn environment in GaAs. Specifically, these results confirm our original assumption that Sn is indeed tetrahedrally coordinated with As in GaAs (i.e., substitutional on Ga sites). There is no evidence for clusters or microprecipitates, in contrast to the Mössbauer results (Williamson et al., 1986).

The mean Δr found from both fits is -0.03 Å. Using that value of Δr and the nn Sn-As distance in the standard (2.60 Å), we find that the nn distance is 2.57 ± 0.02 Å. This is 0.12 Å larger than the Ga-As separation of 2.45 Å (found from the lattice constant). The Sn-As bond length calculated from the tetrahedral radii of Sn (1.40 Å) and As (1.18 Å) (Kittel, 1976) is 2.58 Å, which is consistent with our results. The dilation is also consistent with the difference

of 0.14 Å in the tetrahedral radii of Sn and Ga (1.26 Å). Note that the dilation is not expected to reflect completely the difference in tetrahedral radii since it is accompanied by considerable lattice strain.

A comparable result was obtained for Te-doped GaAs by Greaves et al. (1986). Those authors found that the Te-Ga bond was 0.13 Å longer than the As-Ga bond, which is slightly less than the difference one finds from the tetrahedral radii of Te (1.32 Å) and As (1.18 Å).

EXAFS Results for Sn DX Centers in $Ga_{0.7}Al_{0.3}As$

It is well established that DX centers are the dominant species in n-type $Ga_{1-x}Al_xAs$ for $x > 0.22$ in the dark at low temperatures. EXAFS data were taken for this Sn state in $Ga_{0.7}Al_{0.3}As$ sample described earlier. To obtain this Sn state, the sample was cooled in the dark from room temperature to ∿80 K in approximately 1 minute.

42 scans were taken, but only 11 were good enough to be added together. The resulting spectra are presented in figures 19 and 20, which show the ratio I_f/I_1 and the $k\chi$, respectively. The threshold energy (E_{th}) varied from 29200.8 to 29206.8 for the added sets. The parameters used for the extraction of the EXAFS $k\chi$ and Fourier transformation are presented in table 9. The 2 eV difference in threshold energy between this sample and GaAs:Sn may or may not be

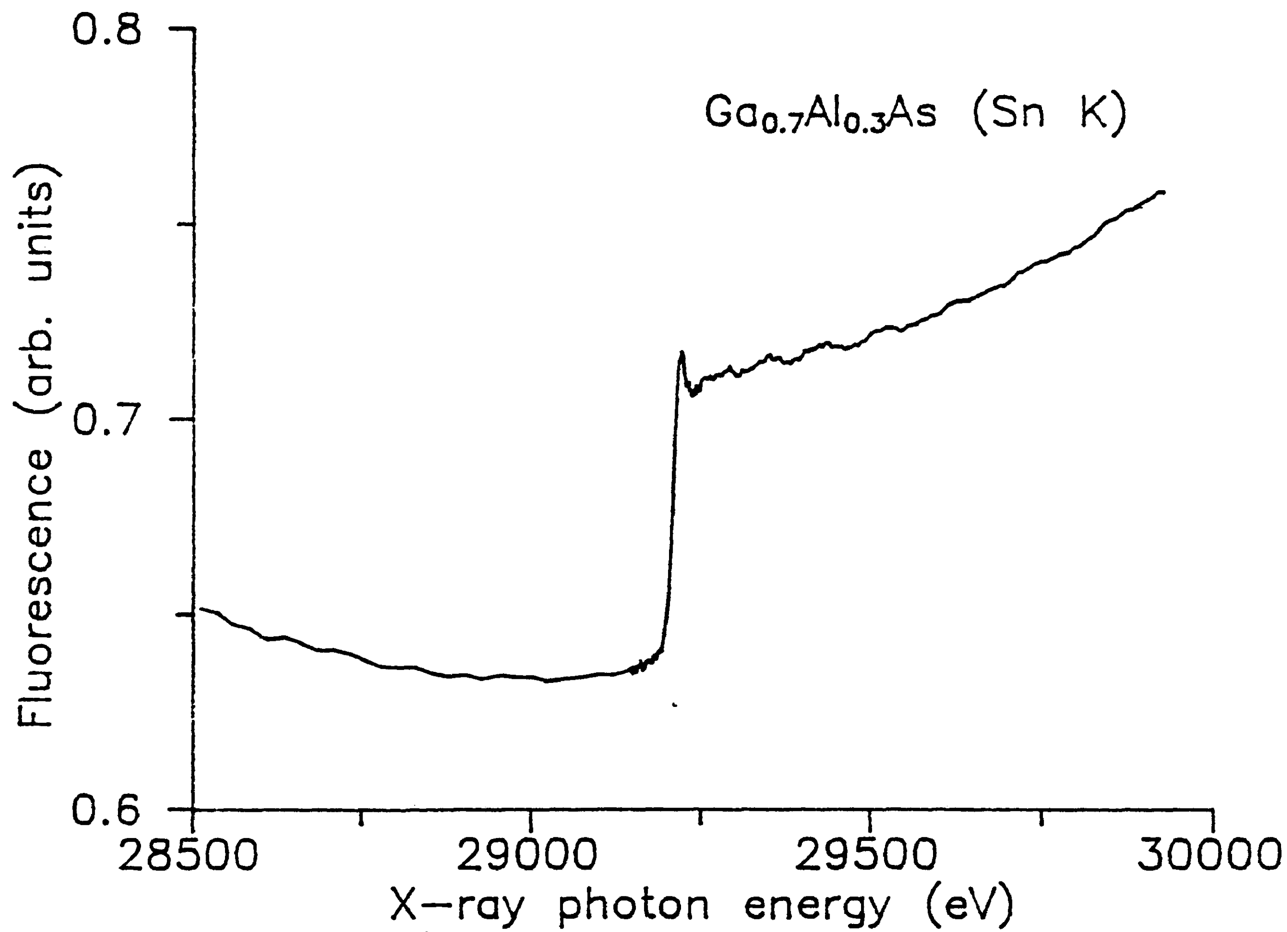

Figure 19. Sn K-shell fluorescence yield of $Ga_{0.7}Al_{0.3}As$:Sn as function of the incident photon energy.

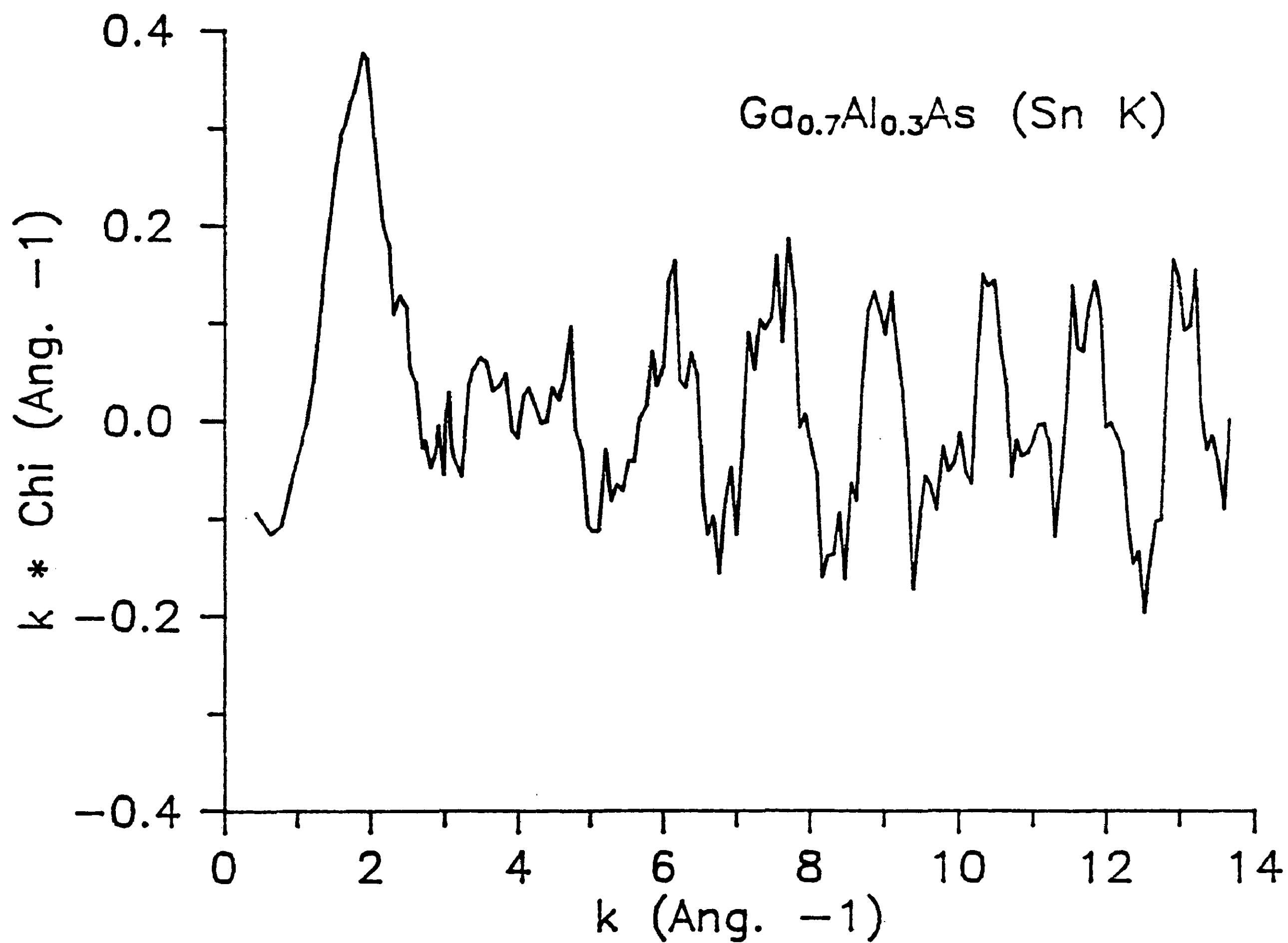

Figure 20. EXAFS oscillations $k\chi(k)$ on the Sn K-shell fluorescence of $Ga_{0.7}Al_{0.3}As$:Sn as function of the photoelectron momentum k.

Table 9. Parameters used for extracting $k\chi$ for $Ga_{0.7}Al_{0.3}As:Sn$.

Energy ranges (eV)

Experimental Range	29175.37		29214.02
Pre-edge fit	29175.37	-	29118.52
Post-edge fit	29216.30	-	29918.90
Edge fit	29200.38	-	29211.75
Final fit	29229.94	-	29921.18

Order final fit	7	
Edge energy (eV)	29206.5	
Edge height	0.071	
Window for FT ($Å^{-1}$)	2.67	12.81
σ for FT ($Å^{-1}$)	0.5	

significant. The edge heights are approximately equal in the two samples, indicating similar concentrations of Sn atoms. Differences in edge height could also arise from variations in thickness or in the irradiated areas of the samples.

The FT of $k\chi$ is shown in figure 21. By comparing $k\chi$ from this sample with the one from GaAs, it can be seen that they are similar except for noise. The Sn nn peaks in ϕ are very similar in $ZnSnAs_2$, GaAs:Sn, and $Ga_{0.7}Al_{0.3}As$:Sn, both in amplitude and in phase. This a qualitative indication that the nn environment of the Sn atoms is similar in the three samples.

The peak function, ξ_{Sn-As}, extracted from $ZnSnAs_2$ was used to fit the nn peak in this spectrum. Both one and two-peak fits were carried out. The coordination number was fixed at four (i.e., amplitude fixed at one). The one-peak fit result is $\Delta r = -0.012$ Å and $R = 0.041$ without a shift in the threshold energy (see table 10). If the threshold energy of the sample is shifted in steps of 0.5 eV, the minimum residual error $R = 0.029$ occurs at $\Delta E_0 = -1.5$ eV and $\Delta r = -0.017$ Å. When the amplitude is allowed to vary, the best fits indicate a coordination number of 4 ± 0.4. Note that the nn peak about Sn in this sample has approximately the same width as the one in the standard.

To confirm these results, one-peak fits were also carried out using GaAs:Sn as a standard. The best fits

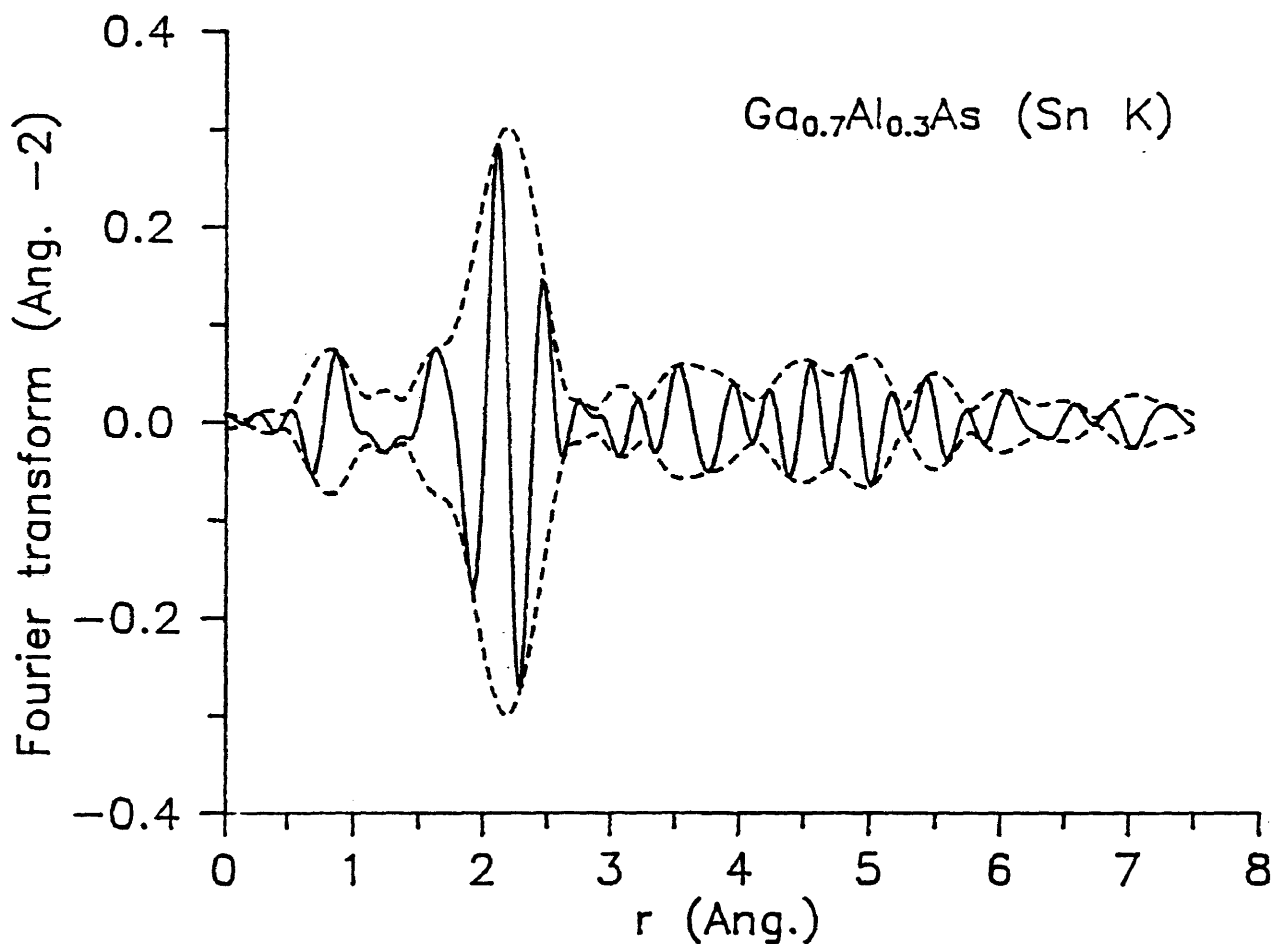

Figure 21. Magnitude (dashed lines) and real part (solid line) of the Fourier transform of $Ga_{0.7}Al_{0.3}As$:Sn $k\chi$ obtained by using a (2.67,12.81) $Å^{-1}$ square window broadened by a Gaussian of halfwidth 0.5 $Å^{-1}$.

Table 10. Structural parameters of Sn in $Ga_{0.7}Al_{0.3}As$: One-peak fits.

Standard : $ZnSnAs_2$

Range of comparison : 1.8 2.56 Å

ΔE_o	Amplitude	Δr (Å)	$\Delta\sigma^2$ (Å^2)	R
0	1	-0.012	-0.0002	0.041
-1.5	1	-0.017	-0.0002	0.029

Standard : GaAs:Sn

ΔE_o	Amplitude	Δr (Å)	$\Delta\sigma^2$ (Å^2)	R
0	1	0.024	0.0000	0.024
3	1	0.014	0.0000	0.008

ARTHUR LAKES LIBRARY
COLORADO SCHOOL of MINES
GOLDEN, COLORADO 80401

(summarized in table 10) showed a difference of 0.014 Å between the nn distances, consistent with the results of the previous fit, and did not reveal any significant relative broadening.

Two-peak fits were done using the two standards mentioned above. The results are shown in table 11. As before, the two peaks are so close to one another as to be regarded as a single asymmetric peak. The quality of the fits leads us to conclude that they best represent the environment of Sn dopants in this sample. The fits using $ZnSnAs_2$ as a standard showed no mean shift, or a nn distance of 2.60 ± 0.02 Å. The fits using the peak function extracted from GaAs:Sn data showed a mean $\Delta r = 0.03$, also indicating a nn distance of 2.60 ± 0.02 Å.

These fits lead us to the conclusion that Sn dopant atoms are tetrahedrally coordinated with As in $Ga_{0.7}Al_{0.3}As$ and that the Sn-As bond length is 2.60 ± 0.02 Å. This represents an increase of 0.03 Å in the Sn-As bond length in the DX center relative to the shallow donor state of the Sn atoms in the samples under study. This result suggests a small lattice relaxation for the DX center.

Recall that Mizuta and Kitano (1988) (see also Kitano and Mizuta, 1987) found no significant lattice distortion at the Se DX center from their EXAFS experiments on Se-doped $Ga_{0.62}Al_{0.38}As$. Their results are not conclusive for the

Table 11. Structural parameters of Sn in $Ga_{0.7}Al_{0.3}As$: two-peak fits.

Standard : $ZnSnAs_2$

Range of comparison: 1.8 - 2.56 Å

ΔE_0	Amplitude	Δr (Å)	$\Delta\sigma^2$ (Å^2)	R
-0.5	0.75	0.030	-0.003	0.009
	0.25	-0.085	-0.007	
-0.5	0.5	0.060	-0.0045	0.010
	0.5	-0.062	-0.0056	

Standard : GaAs:Sn

Range of comparison: 1.8 2.56 Å

ΔE_0	Amplitude	Δr (Å)	$\Delta\sigma^2$ (Å^2)	R
0.0	0.75	0.001	-0.004	0.006
	0.25	+0.127	-0.006	
0.0	0.5	0.093	-0.004	0.006
	0.5	-0.024	-0.005	

following reasons: Se has a complicated nn environment (substitutes for As); the high concentration of Se donors (1 to $3x10^{19}$ cm^{-3}), which probably results in clustering or precipitates. These concentrations are a factor of 2 to 6 larger than in our samples. In addition, their data is considerably noisier than ours and they used a smaller range of k space in their analysis (2.8-9.2 $Å^{-1}$, compared with our transform range of 2.67-12.81 $Å^{-1}$).

Recall that the MES results suggest a distortion from T_d symmetry at the donor site (Gibart et al., 1988). We see no evidence of a distortion affecting the bond lengths. It is possible, however, to explain the MES results with a distortion of bond angles, breaking the T_d symmetry at the donor site but not affecting the bond lengths. The present EXAFS experiments would not reveal such distortion because they probe the spherical average of the pair distribution function.

A $Ga_{0.7}Al_{0.3}As$ single crystal sample was also characterized for the three sample conditions of interest: in the dark, under infrared light and in dark after annealing. These experiments were designed to reveal any local lattice configuration changes between the relaxed and unrelaxed (ionized) DX states. These EXAFS data are, however, contaminated with a varying background signal which is believed to be due to the diffraction from this sample.

This background made the extraction of reliable structural information impossible.

Summary

We have measured the Sn K-edge fluorescence EXAFS of GaAs and $Ga_{0.7}Al_{0.3}As$ doped with $5x10^{18}$ cm^{-3} Sn. These samples are at least a factor of two to six more dilute than others have measured. After an extensive comparison between the Sn nn peaks of $ZnSnAs_2$ and the two Sn-doped samples we conclude that:

- The Sn atoms are tetrahedrally coordinated by As atoms (i.e., occupy the group III sites) in both GaAs and $Ga_{0.7}Al_{0.3}As$.
- The Sn-As bond length is 2.57 ± 0.02 Å in GaAs, which is consistent with the tetrahedral radii of Sn and As. This corresponds to a dilation of 0.12 Å about Sn in GaAs, relative to the Ga-As bond length.
- The Sn-As bond length is 2.60 ± 0.02 Å in $Ga_{0.7}Al_{0.3}As$. This dilation is slightly larger than for GaAs.
- The peak-shape is not a simple Gaussian in either case.
- The Sn-As bond length associated with the DX center in $Ga_{0.7}Al_{0.3}As$ is 0.03 ± 0.02 Å larger than that associated with the shallow donor state of Sn in GaAs. This is an indication of a small dilatational lattice relaxation at the DX center.

RECOMMENDATIONS FOR FURTHER WORK

This study found no evidence for a large lattice relaxation associated with the occupied DX center. It is difficult to understand, however, how a SLR model can account for a large photoionization threshold for this defect. The possible implications of this are:

i) the DX center has lower photoionization threshold in our samples. It would be valuable to measure the photoionization thresholds of the Sn DX centers in the samples used for this EXAFS study, or in similarly produced samples, by measuring the onset of the PPC.

ii) the Sn atoms may not be in the DX state during our measurement. They may have been ionized by the x rays. It would be useful to study the effect of 29 keV x rays on the DX state at various temperatures below 80 K by measuring the conductivity of the sample before, during, and after exposure to the x rays.

In this study, we compared relaxed DX centers in $Ga_{0.7}Al_{0.3}As$ with the shallow donor Sn environment found in GaAs. It is also possible to compare the relaxed DX center directly with the ionized donor in the same sample (i.e., $Ga_{0.7}Al_{0.3}As$) by exciting a majority of the donors into the PPC state. Such a direct comparison should be most sensitive to small changes in Sn environment. This experiment should

be tried again. Similarly, it would also be valuable to characterize the PPC state by MES and compare those results directly with those from the DX state in the same sample.

Recently, it was argued that the DX center localizes two electrons and becomes a negatively charged entity in the ground state (Chadi and Chang, 1988). The implications of such a state for the interpretation of the EXAFS data should be considered.

REFERENCES CITED

Chadi D.J., Chang K.J., "Theory of the Atomic and Electronic Structure of DX centers in GaAs and $Al_xGa_{1-x}As$ Alloys", Phys. Rev. Lett. **61**, 873 (1988).

Chand N., Henderson T., Kelm J., Masselink W.T., Fisher R., Chang Y., Morkoc H., "Comprehensive analysis of Si-doped $Al_xGa_{1-x}As$ ($x = 0$ to 1): theory and experiments", Phys. Rev. **B30**, 4481 (1984).

Craford M.G., Stillman G.E., Rossi J.I., Holonyak N. Jr, "Effect of Te and S donor levels on the properties of $GaAs_{1-x}P_x$ near the direct-indirect transition", Phys. Rev. **68**, 867 (1968).

Eljani B., Köhler K., N'Guessan K., Bel Hadj A., Gibart P., "Shallow and deep donors in n-type $Ga_{1-x}Al_xAs$ grown by metallorganic vapor-phase epitaxy", J. Appl. Phys. **63**, 4518 (1988).

Gibart P., Williamson D.L., Eljani B., Basmaji P., "^{119}Sn Mössbauer study of shallow and deep states of Sn in $Ga_{1-x}Al_xAs$", Phys. Rev. **B38**, 1885 (1988).

Gibart P., Williamson D.L., Moser J., Basmaji P., "Pressure-induced shallow-to-deep donor state transition in ^{119}Sn-doped GaAs observed by Mössbauer spectroscopy", 1989 (submitted to Phys. Rev. Lett.).

Greaves G.N., Halfpenny P.J., Lamble G.M. and Roberts K.J., "The structural environment of Te dopants in GaAs using EXAFS in fluorescence mode", J. Phys. **C8**, 901 (1986).

Hayes T.M., Boyce J.B., "Extended x-ray absorption fine structure spectroscopy ", in Solid State Physics **37**, ed. by Ehrenreich, H., Seitz, F., and Turnbull D. (Academic Press, New York, 1982), 173-351.

Hayes T.M., Sen P.N., Hunter S.H., "Structure determination in real space: Ge", J. Phys. C: Solid State Phys. **9**, 4357 (1976).

Henning J.C.M., Ansems J.P.M., "A new model of deep donor centers in $Al_xGa_{1-x}As$", Semicond. Sci. Technol. **2**, 1 (1987).

Henry C.H., Lang D.V., "Nonradiative capture and

recombination by multiphonon emission in GaAs and GaP", Phys. Rev. **B15**, 989 (1977).

Jaffe J.E., and Zunger A. , "Theory of the band-gap anomalies in ABC_2 chalcopyrite semiconductors", Phys. Rev. **B29**, 1882 (1984).

Khachaturyan K.A., Weber E.R., "Quasipolaron model of deep donor in n-AlGaAs and other III-V and II-VI semiconductors" (unpublished).

Khachaturyan K.A., Weber E.R., Kaminska M., "Persistent photoconductivity due to negative U centers in compound semiconductors", in Proc. 15th Int. conf. on Defects in Semiconductors, August 22-26, 1988 Budapest (in press).

Kitano T., Mizuta M., "Fluorescence EXAFS study of AlGaAs doped with Se donor impurities", Jpn. J. Appl. Phys. **26**, L1806 (1987).

Kittel C., "Introduction to Solid State Physics", 6th ed. (Wiley, New York, 1976).

Lang D.V., "DX Centers in III-V Alloys", in Deep Centers in Semiconductors, ed. by S.T. Pantelides (Gordon Beach, New York, 1985), 489-537.

Lang D.V., Logan R.A., "Large-Lattice-Relaxation Model for Persistent-Photoconductivity in Compound Semiconductors", Phys. Rev. Lett. **39**, 653 (1977).

Lang D.V., Logan R.A., Jaros M., "Trapping characteristics and a donor-complex (DX) model for the persistent-photoconductivity trapping center in Te-doped $Al_xGa_{1-x}As$", Phys. Rev. **B19**, 1015 (1979).

Lannoo M., Bourgoin J., "Point defects in semiconductors I: Theoretical Aspects", Springer-Verlag series in Solid-State Sciences, (Springer-Verlag, Berlin Heidelberg, 1981).

Lee P.A., Citrin P.H., Eisenberger P., Kincaid B.M, "Extended x-ray absorption fine structure-its strengths and limitations as a structural tool", Rev. Mod. Phys. **53**, 769 (1981).

Maude D.K., Portal J.C., Dmowski L., Foster T., Eaves L., Nathan M., Heiblum M., Harris J.J., Beall R.R.,

"Investigation of the DX center in Heavily Doped n-type GaAs", Phys. Rev. Lett. **59**, 815 (1988).

Mizuta M., Kitano T., "Small lattice relaxation at the DX center as studied by extended x-ray absorption fine structure on Se-doped AlGaAs", Appl. Phys. Lett. **52**, 126 (1988).

Mizuta M., Tachickawa M., Kukimoto H., Minomura S., "Direct evidence of DX centers being a substitutional donor in AlGaAs alloy system", Jpn. J. Appl. Phys. **24**, L143 (1985).

Mizuta M., Mori K., "Investigation of the DX center in the indirect $Al_xGa_{1-x}As$ alloy", Phys. Rev. **B37**, 1043 (1988).

Morgan T.N., "Theory of the DX center in $Al_xGa_{1-x}As$ and GaAs crystals", Phys. Rev. **B34**, 2664-2669 (1986).

Narayanamurti V., Logan R.A., Chin M.A., "Symmetry of Donor-Related Centers Responsible for Persistent Photoconductivity in $Al_xGa_{1-x}As$", Phys. Rev. **B43**, 1536 (1979)

Nelson R.J., "Long-lifetime photoconductivity effect in n-type GaAlAs", Appl. Phys. Lett. **31**, 351 (1977).

Oshiyama A., Ohnishi S., "DX center: Crossover of deep and shallow states in Si-doped $Al_xGa_{1-x}As$", Phys. Rev. **B33**, 4320 (1986).

Saxena A.K., "The conduction band structure and deep levels in $Ga_{1-x}Al_xAs$ alloys from a high-pressure experiment", J. Phys. C: Solid State Phys. **13**, 4323 (1980).

Small P.R.G, "The Atomic-Scale Structure of Dilute Tin in Aluminum", Thesis T-3607, Colorado School of Mines, 1989.

Tachickawa M., Fujisawa T., Kukimoto H., Shibata A., Oomi G., Minomura S., "Observation of persistent-photoconductivity due to DX center in GaAs under hydrostatic pressure", Jpn. J. Appl. Phys. **24**, L893 (1985).

Theis T.N., "The DX center in GaAs and $Ga_{1-x}Al_xAs$", Proc. 3rd Int. Conf. on Shallow Impurities in Semiconductors, August 10-12 (1988), Linkoeping, Sweden.

Theis T.N., Kuech T.F., Palateer T.F., Mooney P.M., "Far infrared spectroscopy of silicon donors in $Ga_{1-x}Al_xAs$", in Proc. Int. Conf. on GaAs and Related Compounds, Inst. Phys. Conf. series **74**, 241 (1984).

Theis T.N., Parker D.B., Solomon P.M., Wright S.L. "Hot-electron capture to DX centers in $Al_xGa_{1-x}As$ at low Al mole fractions", Appl. Phys. Lett. **49**, 1542 (1986).

Theis T.N., Mooney P.M., Wright S.L., "Electron localization by a metastable donor level in n-GaAs: a new mechanism limiting the free carrier density", Bull. Am. Phys. Soc. **32**, 554 (1987).

Toyozawa Y., Shinozuka Y., "Stability of an electron in deformable lattice -force range, dimensionality and potential barrier-", J. Phys. Soc. Jpn. **48**, 472 (1980).

Troxel T., SSRL Report #11B-85-V4, (1985).

Uchida U., Kobayachi K.L.I., Nakashima H., "Electrical properties of DX center In $Ga_{1-x}Al_xAs$ and its bond reconstruction model", Jpn. J. Appl. Phys. **27**, L928 (1985).

Williamson D.L., "Mössbauer spectroscopy of Sn-doped GaAs grown by liquid-phase epitaxy", J. Appl. Phys. **60**, 3466 (1987).

Yamaguchi E., "The origin of DX center in $Al_xGa_{1-x}As$", Jpn. J. Appl. Phys. **25**, L643 (1986).

Yamaguchi E., "Theory of the DX centers in III-V semiconductors and (001) superlattices", J. Phys. Soc. Jpn. **56**, 2835 (1987).

APPENDIX A

Calculation of the resolution of the double crystal mononochromator.

The resolution of the monochromator is defined as :

$$\frac{\Delta E}{E} = \cot(\theta)\ \Delta\theta + \left[\frac{\Delta E}{E}\right]_{crystal}$$

where $\Delta\theta$ is the spread in the Bragg angle and the second term is intrinsic to each crystal. The only spread we took into account was the one due to source and slit widths defined as:

$$\Delta\theta = \frac{w_s + w}{d}$$

where w_s is the vertical source size, w is the entrance slit size, and d is the distance between the source and the slit. The parameters listed in table 3 permit the calculation of the resolution as function of energy and the other parameters as was done in table 3.

APPENDIX B

Evaluation of sample thickness from the transmitted intensity.

This procedure is based upon calculating the product $z_s \mu_s$ from the $Log(I_1/I_2)$ spectrum of the sample at a given photon energy E (see experimental technique section for equations relating this expressions). The absorption coefficient of the sample (μ_s) is then calculated from the tabulated mass-absorption coefficient of the elements constituting the sample, and the thickness deduced. For multi-element compound like $Ga_{1-x}Al_xAs$, the mass absorption coefficient is given by:

$$(\mu/\rho\ ) = \sum_i C_i\ (\mu/\rho)_i$$

where (μ/ρ) is the mass absorption coefficient and C_i is the mass percentage of each element in the compound. For $Ga_{1-x}Al_xAs$ the coefficients C_i were found to be:

$$C_{Ga} = (1-x)\ M_{Ga}/M,$$

$$C_{Al} = x\ M_{Al}/M,$$

and $$C_{As} = M_{As}/M\ ,$$

where $M = (1-x)\ M_{Ga} + x\ M_{Al} + M_{As}$ is the molar mass of the compound and the M_i are the molar masses of the elements.

APPENDIX C

Calculation of the nearest-neighbor distances.

a. Tetrahedral coordination:

$$r_{nn} = a \frac{\sqrt{3}}{4}$$

b. Octahedral coordination:

$$r_{nn} = \frac{a}{2}$$

where a is the lattice constant. These equations are derived under the approximation that the atoms are hard spheres in contact.

For the case of Sn in $ZnSnAs_2$, an alternative formula suggested by Jaffe and Zunger (1984) was used:

$$r_{nn} = a \sqrt{(u-1/2)^2 + (1+\eta^2)/16} \quad ,$$

where $\eta = c/2a$ and $u = 0.23$; $u - 1/4$ and η measure the bond alteration in the system and the tetragonal deformation respectively. This equation yields an nn distance in good agreement with the one found from our EXAFS measurements using SnAs as a standard (see data analysis section).